JOURNAL OF PETROLOGY | VOLUME 49 | NUMBER 6 | PAGES 1161–1185 | 2008 | doi:10.1093/petrology/egn021

The Titanomagnetite–Ilmenite Equilibrium: New Experimental Data and Thermo-oxybarometric Application to the Crystallization of Basic to Intermediate Rocks†

URSULA SAUERZAPF, DOMINIQUE LATTARD*, MICHAEL BURCHARD AND RALF ENGELMANN

MINERALOGISCHES INSTITUT, RUPRECHT-KARLS-UNIVERSITÄT HEIDELBERG, INF 236, D-69120 HEIDELBERG, GERMANY

RECEIVED SEPTEMBER 10, 2007; ACCEPTED MARCH 27, 2008
ADVANCE ACCESS PUBLICATION MAY 7, 2008

Although the titanomagnetite–ilmenite thermo-oxybarometer has been widely used to provide information on temperature and oxygen fugacity during magmatic and metamorphic processes, the available formulations yield unsatisfactory results; for example, at high temperature and low to moderate fO_2 (i.e. in conditions relevant to crystallization in basic and intermediate rocks). We present a new version of this thermo-oxybarometer based on numerical fits of a large experimental dataset comprising new results in the Fe–Ti–Al–Mg–O system and those of literature studies. Our new subsolidus experimental results at temperatures in the range 1100–1300°C under low to moderate fO_2 conditions show that the addition of Mg and/or Al in the concentration ranges that are usual in Fe–Ti oxides from basic magmatic rocks can be accommodated by simple projections. We have taken advantage of this fact and performed numerical fits to generate empirical formulations. With the resulting expressions we can retrieve temperature values from X'_{usp} and X'_{ilm} (projected mole fractions) of titanomagnetite–ilmenite$_{ss}$ pairs and fO_2 values from X'_{usp} and T. The present thermo-oxybarometer model is designed for assemblages of titanomagnetite and hemoilmenite (with the $R\bar{3}$ space group), with the usual low Al_2O_3, Cr_2O_3, MgO and MnO contents (less than about 6 wt %), which equilibrated at high temperatures ($T \geq 800°C$) and low to moderate oxygen fugacities ($-4 < \Delta NNO < +2$, where NNO is the nickel–nickel oxide buffer). Tests of our model by using the compositions of titanomagnetite–ilmenite$_{ss}$ pairs in products of liquidus experiments conducted at known T–fO_2 conditions (literature data and new results) show that the calculated values reproduce the experimental ones within ±70°C, and in most cases within ±50°C. The estimates of the oxygen fugacity are mostly within ±0·4 log units. This is a significant improvement compared with the previous models.

KEY WORDS: *Fe–Ti oxides; geothermometry; ilmenite; oxygen fugacity; titanomagnetite*

INTRODUCTION

The equilibrium between the iron–titanium oxide minerals titanomagnetite and ilmenite has been widely used to estimate both temperatures and oxygen fugacities in igneous and metamorphic rocks of the Earth, the Moon or other terrestrial planets. Buddington & Lindsley (1964) introduced the titanomagnetite–ilmenite thermo-oxybarometer and provided the first calibration based on the experimental results of Lindsley (1962, 1963) in the Fe–Ti–O system. The thermometer is based on the temperature-dependent exchange of $Fe^{2+} + Ti^{4+}$ for 2 Fe^{3+} between titanomagnetite (solid solution between the magnetite and the ulvöspinel endmembers) and ilmenite (solid solution between the

*Corresponding author. Telephone: +49 6221 544810. Fax: +49 6221 544805. E-mail: dlattard@min.uni-heidelberg.de

†This contribution is dedicated to the memory of Eduard Woermann (1929–2008), Professor at the University of Aachen (Germany), who generously shared with us his profound knowledge on oxide minerals and redox phase relations.

© The Author 2008. Published by Oxford University Press. All rights reserved. For Permissions, please e-mail: journals.permissions@oxfordjournals.org

Downloaded from https://academic.oup.com/petrology/article/49/6/1161/1490007 by guest on 16 August 2022

hematite and the ilmenite endmembers) according to the reaction

$$Fe_2TiO_4\ (\text{ulvöspinel}) + Fe_2O_3\ (\text{hematite}) = FeTiO_3\ (\text{ilmenite}) + Fe_3O_4\ (\text{magnetite}). \quad (1)$$

The oxybarometer is based on iron redox equilibria, which may be formulated by the magnetite–hematite oxygen buffer equilibrium or by an equilibrium involving the Ti-rich endmembers of the two Fe–Ti oxide series; that is,

$$6FeTiO_3\ (\text{ilmenite}) + 2Fe_3O_4\ (\text{magnetite}) = 6Fe_2TiO_4\ (\text{ulvöspinel}) + O_2. \quad (2)$$

Compositional departures from the Fe–Ti–O system were accounted for in an empirical manner (e.g. Buddington & Lindsley, 1964; Carmichael, 1967; Anderson, 1968; Lindsley & Spencer, 1982; Stormer, 1983). Numerous attempts were made to model the exchange and redox reactions that govern this thermo-oxybarometer (e.g. Rumble, 1970; Powell & Powell, 1977; Spencer & Lindsley, 1981; Andersen & Lindsley, 1988; Ghiorso & Sack, 1991*a*).

There are two current popular versions of the thermo-oxybarometer: one is included in the QUILF package (Frost & Lindsley, 1992; Lindsley & Frost, 1992; Andersen *et al.*, 1993) and utilizes the solution models of Andersen & Lindsley (1988) and Andersen *et al.* (1991), and the other is the formulation of Ghiorso & Sack (1991*a*), which is based on the thermodynamic analysis of the same researchers and combines the solution models of Ghiorso (1990) and Sack & Ghiorso (1991*a*, 1991*b*). Lindsley & Frost (1992) have emphasized, however, that their formulation is not designed to be used for equilibria at oxygen fugacities higher than two log bar units above those of the fayalite–magnetite–quartz equilibrium (FMQ) (i.e. at $\Delta FMQ > 2$ or $\Delta NNO > 1{\cdot}3$). Unfortunately, the formulation of Ghiorso & Sack (1991*a*) also strongly overestimates both temperature and fO_2 at such relatively high fO_2 conditions. (Evans & Scaillet, 1997; Scaillet & Evans, 1999; see also Lattard *et al.*, 2005, fig. 1). However, both formulations underestimate the temperature for conditions relevant to magmatic crystallization in basalts (see Lattard *et al.*, 2005, fig. 1).

It has become clear that the shortcomings of the two thermo-oxybarometer models largely originate from the paucity of calibration data at high temperatures but also—for all temperatures—at oxygen fugacities far from those of the FMQ buffer. Two recent experimental studies (Lattard *et al.*, 2005; Evans *et al.*, 2006) have now filled these gaps by providing a large set of experimental data in the critical T–fO_2 ranges. Evans *et al.* (2006) have also considered the effect of additional components on the Fe–Ti oxide compositions at 800 and 900°C at relatively high oxygen fugacities.

In this paper we present new experimental data on the compositions of coexisting titanomagnetite and ilmenite solid solution in the Fe–Ti–O system at 950°C and on Mg-bearing and/or Al-bearing Fe–Ti oxide assemblages at 1100–1300°C. These new results complement our dataset at high temperatures (1000–1300°C) in the simple Fe–Ti–O system (Lattard *et al.*, 2005) and the results of Evans *et al.* (2006) in the Fe–Ti–Al–Mg–Mn–O system at 800 and 900°C. We show that the addition of minor components in the concentration ranges that are usual in Fe–Ti oxides from basic magmatic rocks can be, to a first approximation, accommodated by simple projections. We have performed numerical fits to available experimental data with the aim of generating a simple empirical formulation of the titanomagnetite–ilmenite thermo-oxybarometer for temperatures in the range 800–1300°C, under reduced to moderately oxidized conditions. We have tested this empirical formulation both with synthetic and natural Fe–Ti oxide pairs and we shall show in the following that the results are encouraging.

We refer the readers to the review of Lindsley (1991) and to our recent paper (Lattard *et al.*, 2005) for summaries of the experimental studies that unravelled the sub-solidus phase relations in the Fe–Ti–O system.

EXPERIMENTAL AND ANALYTICAL TECHNIQUES

All experiments reported in the following discussion were designed to produce equilibrium pairs of titanomagnetite (Tmt) and ilmenite–hematite solid solution (Ilm_{ss}) at 1 bar pressure under various oxygen fugacity conditions. Three types of experiments were performed: (1) sub-solidus syntheses at 1100, 1200 or 1300°C from oxide mixtures in the Fe–Ti–Al–Mg–O system; (2) sub-solidus re-equilibration experiments at 950°C in evacuated silica-glass ampoules on products of previous syntheses in the Fe–Ti–O system; (3) crystallization experiments from a basic liquid at temperatures in the range 1050–1080°C.

All experiments were performed in vertical quench furnaces. The temperature was measured before and after the runs with a type S ($Pt–Pt_{90}Rh_{10}$) thermocouple calibrated against the melting point of silver (960·8°C) and gold (1064·18°C; ITS 90).

Sub-solidus syntheses in the Fe–Ti–Mg–Al–O system

The sub-solidus syntheses reported here were aimed at producing assemblages of Tmt and Ilm_{ss} with low Mg and/or Al contents comparable with those observed in magmatic Fe–Ti oxide minerals. The experiments were performed at 1100, 1200 or 1300°C, under a variety of oxygen fugacities (ΔNNO range: +0·7 to −4·6), which were in most cases fixed by $CO–CO_2$ gas mixtures.

Downloaded from https://academic.oup.com/petrology/article/49/6/1161/1490007 by guest on 16 August 2022

Table 1: Chemical compositions of starting materials: eight-component SC47-P glass and oxide–metal starting mixtures in the Fe–Ti–Al–Mg–O system

wt %	SC47-P	F70A2	IT60A2	F59.5A5.5	F70M2	IT60M2	F57.4M10	IT70M1A1	IT60M1A1
SiO_2	48·97 (27)								
TiO_2	4·91 (8)	29·4	40·9	38·8	29·4	40·9	41·2	30·9	40·9
Al_2O_3	10·89 (12)	2·0	2·1	4·3				1·0	1·0
Fe_2O_3	18·83 (41)*	68·6	47·0	56·9	68·6	47·0	55·6	55·2	47·0
Fe°			10·0			10·0		11·8	10·0
MgO	4·26 (6)				2·0	2·1	3·1	1·1	1·0
CaO	8·92 (15)								
Na_2O	2·86 (13)								
K_2O	0·65 (3)								
Total	100·29 (55)	100·0	100·0	100·0	100·0	100·0	99·9	100·0	99·9

In the SC47-P column the first value is the mean and the value in parentheses is 1σ to second decimal place of 100 EMP analyses of the glassy starting material. All other columns list the weighed values of the reagents.
*Total Fe recalculated to Fe_2O_3.

In a few experiments at 1100°C the oxygen fugacity was imposed by a solid-state oxygen buffer enclosed together with the sample in an evacuated SiO_2 glass ampoule.

We chose a few bulk compositions in the two sub-systems Fe–Ti–Mg–O and Fe–Ti–Al–O with 2–4 wt % of either MgO or Al_2O_3, as well as two compositions with about 1 wt % of both minor components (Table 1). The starting mixtures were prepared from TiO_2 (99·9%, Aldrich Chemical Comp. Inc.), Fe_2O_3 (99·9%, Alpha Products), metallic iron (99+%, Heraeus), MgO (99·5%, Ventron) and/or γ-Al_2O_3 (purest, Merck). Metallic iron was first employed in starting mixtures for experiments performed with solid-state oxygen buffers. In this case, the original oxygen content of the sample should be close to that of the run product because of the restricted buffer capacity. Starting mixtures with both Fe° and Fe_2O_3 also proved suitable for some gas mixing experiments because they yielded very homogeneous run products. The reagents were weighed in stoichiometric proportions, ground together and mixed under acetone in an agate mortar, pressed to pellets of 200–300 mg (about 5 mm diameter, 2–5 mm in length) and dried in air at 130°C.

For the solid-state buffer experiments, pellets of sample and buffer material (iron–wüstite or wüstite–magnetite) were inserted in silica-glass tubes, which were evacuated with a rotary vane pump to a vacuum of the order of 10^{-2} mbar prior to sealing. A silica-glass filler rod was used to minimize the internal volume of the ampoule and to separate the sample from the buffer. At the end of the experiments, the silica-glass ampoules were pulled out of the furnace and quenched into water, a procedure that lasted less than 1 min. In all runs referred to in this paper all buffer phases were still present after termination of the experiments; that is, the desired oxygen fugacity was maintained during the whole experiment.

For the gas-mixing experiments, the sample pellets were placed on a grid of platinum wire. As sample and metal share only a very small surface and no melt ever occurs in the samples, negligible Fe loss to the wire but maximum contact of sample with gas mixture can be achieved. High-purity CO (CO >99·97 vol. %) and CO_2 (CO_2 >99·995 vol. %) gases were mixed with electronic valves (Millipore) and allowed to flow from the bottom to the top of the furnace tube (inner diameter 4 cm) at a rate of 200 cm^3/min. The oxygen fugacity was measured after the experiments with an yttria-stabilized zirconia sensor (SIRO2) with air as the reference. The sensor was calibrated at 1300°C against the Ni–NiO (NNO) equilibrium (O'Neill & Pownceby, 1993). At the moderate to low oxygen fugacities reported in the present study (ΔNNO < +1; CO > 1 vol. %), the accuracy of the experimental fO_2 values are estimated at about ±0·2 log unit [for further details see Lattard *et al.* (2005)]. All fO_2 values given for the gas-mixing experiments in the following are those measured with the zirconia sensor. As we also list the CO contents of the gas mixtures, the reader can easily retrieve the fO_2 values from the tables of Deines *et al.* (1974) for comparison.

Run products were generally drop-quenched in water at the bottom of the furnace, a procedure that ensures a very fast cooling (within a few seconds). In a few cases, however, the gas flow was first turned off and the samples were pulled out of the furnace and quenched in water. The whole procedure usually took less than 1 min. In the following discussion this is referred to as 'external quench'.

To approach equilibration as closely as possible in the synthesis products, total run durations were 18–60 h at

Downloaded from https://academic.oup.com/petrology/article/49/6/1161/1490007 by guest on 16 August 2022

1300°C, but up to 330 h (14 days) at 1100°C. These run durations are longer than those applied in the Fe–Ti–O system (see Lattard *et al.*, 2005) because the addition of magnesium and aluminium in the starting materials was expected to slow down the reaction kinetics, which could lead to inhomogeneous samples. Indeed, a few preliminary runs yielded products that contained a few grains of Fe–Al-rich spinel surrounded by zoned Tmt crystals with Al-bearing rims in contact with the Fe–Al spinel. Such Al-enriched regions disappeared if the samples were crushed, re-pelletized and re-run under the same T–fO_2 conditions for at least another 24 h. Consequently, the gas-mixing runs at 1200°C and 1100°C reported here were interrupted through drop-quench after 1 or 2 days, the samples were ground to a powder under acetone, re-pressed to a new pellet and re-run under the same T–fO_2 conditions for at least another 24 h.

Sub-solidus re-equilibration experiments at 950°C *in vacuo* (Fe–Ti–O system)

Our experiments at 950°C under low vacuum were originally designed to re-equilibrate under oxygen-conserving conditions Tmt–Ilm_{ss} assemblages previously synthesized in the Fe–Ti–O system at high temperatures (1100–1300°C) under various oxygen fugacities. The incentive was to estimate the original vacancy concentration of the high-temperature titanomagnetites from the amount of Ilm_{ss} exsolved from Tmt in correlation with the vacancy relaxation at 950°C (see Lattard, 1995; Sauerzapf, 2006). This aspect will not be considered here, but the run products are of interest for the present purpose because they yield data complementary to our series at 1300, 1200, 1100 and 1000°C in the Fe–Ti–O system (Lattard *et al.*, 2005).

The starting samples were fragments (30–100 mg) of pellets synthesized in gas mixing experiments (procedure summarized in the section 'Sub-solidus syntheses in the Fe–Ti–Mg–Al–O system'). These fragments were sealed in evacuated silica-glass ampoules (vacuum of the order of 10^{-2} mbar). The inner volume of the ampoules was minimized by using filling rods of silica-glass. The ampoules were kept in vertical tube furnaces at 950°C for durations (7–37 days), which should be long enough to approach re-equilibration. The samples were quenched by rapid immersion of the ampoules in cold water. Only dry samples were accepted for further investigation. Detailed investigations have shown that the silica-glass ampoules remain gas-tight and evacuated during the whole experiment and the quenching procedure, and that the sample systems can be considered to be closed for all elements including oxygen (Lattard, 1995; Lattard & Partzsch, 2001).

Crystallization experiments from a basic liquid

We have performed a few crystallization experiments to synthesize Tmt–Ilm_{ss} pairs of compositions relevant to Fe–Ti oxide crystallizing from natural basic magmas. These experiments are similar to those conducted by Toplis & Carroll (1995) and the reader is referred to that paper for more experimental details.

The starting material (SC47-P) was a synthetic eight-component glass with a composition corresponding to that of the residual liquid after 40–50% crystallization of a ferrobasaltic composition [near the SCl composition of Toplis & Carroll (1995)]. The starting glass was synthesized from mixtures of oxides (SiO_2, TiO_2, Al_2O_3, Fe_2O_3 and MgO) and carbonates ($CaCO_3$, Na_2CO_3 and K_2CO_3). The mixtures were decarbonated at 800°C in a Pt crucible for 0·5 h, fused at 1400°C in air for 5 h and poured for quenching into a steel mortar. The material was homogenized by repeated grinding and fusing. Its chemical composition is given in Table 1.

Aliquots of 40–60 mg starting material were loaded onto loops of platinum wire using polyvinyl alcohol as a binder. To minimize iron loss from the sample to the platinum wire (e.g. Ford, 1978; Johannes & Bode, 1978) the loops were 'presaturated' with iron by heating them in contact with some starting material at 1300°C under the required oxygen fugacities for 24 h, followed by cleaning in HF.

The samples were first heated at 1150°C or 1140°C; that is, well above the liquidus (see Toplis & Carroll, 1995) for 8–10 h to allow redox equilibration of the melt. They were subsequently cooled to the final temperature (near 1050 or 1082°C) at a constant rate of 3°C/h (to facilitate nucleation and growth of crystals large enough for microprobe analysis) and held at this temperature for 4–12 days to allow re-equilibration. During the whole procedure the CO–CO_2 mixture was kept to the value corresponding to the oxygen fugacity at the end temperature. Runs were terminated by drop-quench into water. The run durations were of the same order as those of comparable subliquidus experiments in the literature (e.g. Toplis & Carroll, 1995) and should ensure at least a reasonable approach to equilibration at the final temperature.

Identification and chemical analysis of the run products

All run products were carefully characterized using optical microscopy, X-ray powder diffraction, back-scattered electron (BSE) images from a scanning electron microscope (SEM) and chemical analyses with the electron microprobe (EMP).

The EMP, a Cameca SX-5l, was operated at an acceleration voltage of 15 kV and a beam current of 20 nA. Counting times were 20 s on peak and twice 10 s on background. The standards used were synthetic hematite (for Fe), rutile (for Ti), periclase (for Mg) and gahnite (for Al). The raw data were corrected with the 'PAP' software (Pouchou & Pichoir, 1985). To avoid possible instrumental drift, the standardization was checked at least every 2 h. If the

Downloaded from https://academic.oup.com/petrology/article/49/6/1161/1490007 by guest on 16 August 2022

measurements could not be reproduced within less than 1%, a new standardization was performed.

After recasting Fe to Fe^{2+} and Fe^{3+} or Ti to Ti^{4+} and Ti^{3+} on the basis of ideal stoichiometry (i.e. four oxygens and three cations for Tmt, but three oxygens and two cations for Ilm_{ss}), analysis totals range, with few exceptions, between 99 and 100·5 wt %. Repeated analyses on unzoned grains show that the precision of the analyses is excellent [1σ standard deviations for the Ti/(Ti + Fe) values ≤0·5% relative]. The accuracy is also satisfactory, as shown by analyses on a single-phase, very homogeneous ilmenite sample, which yielded Ti/(Ti + Fe) per cent values less than 0·35 at. % different from the bulk composition. As already reported by Lattard *et al.* (2005), analyses performed by D. H. Lindsley at Stony Brook (using a natural ilmenite standard) on two of our Ti-rich Tmt–Ilm_{ss} run products produced only slightly higher Ti/(Ti + Fe) per cent values (difference ≤0·5 at. %). Therefore we think it safe to estimate the accuracy for all compositions at ±0·005 for the Ti/(Ti + Fe) values, which translates into ±0·015 for X_{usp} and ±0·010 for X_{ilm}.

EXPERIMENTAL RESULTS

Products of sub-solidus re-equilibration experiments at 950°C in the Fe–Ti–O system

After annealing at 950°C the samples consist of polycrystalline, roughly equigranular aggregates of Tmt and Ilm_{ss}, with a grain size similar to that of the starting samples (i.e. around 10–50 μm). In nearly all annealed samples, however, the Tmt crystals display exsolution textures in the form of ilmenite lamellae oriented in the {111} planes of the spinel and of ilmenite rims around the spinel crystals. As discussed in detail by Lattard (1995), such textures occur when the modal proportion of Ilm_{ss} in the sample increases during annealing under oxygen-conserving conditions, as a result of the shift of the Tmt composition towards stoichiometry (relaxation of the high-temperature cationic vacancies).

Careful EMP measurements on Ilm_{ss} lamellae and rims of suitable size have shown that they have the same chemical composition as the larger grains (Lattard, 1995; Sauerzapf, 2006). More generally speaking, in all samples both Ilm_{ss} and Tmt mineral phases have homogeneous chemical compositions within the crystals and over the whole sample. This is illustrated by the small standard deviations on the values of the mole fractions of the ulvöspinel (X_{usp}) and the ilmenite endmembers (X_{ilm}), as listed in Table 2. These values are calculated from the Ti/(Ti + Fe) values (cation ratios) obtained from the EMP analyses, where

$$X_{usp} = 3\mathrm{Ti}/(\mathrm{Ti} + \mathrm{Fe}) \text{ and } X_{ilm} = 2\mathrm{Ti}/(\mathrm{Ti} + \mathrm{Fe}).$$

A plot of the Ti/(Ti + Fe) values for coexisting Tmt and Ilm_{ss} shows a consistent arrangement of the tie-lines, with no crossing (Fig. 1), independent of the original synthesis temperature (1300, 1200 or 1100°C). This suggests a good approach to equilibrium.

In most cases, re-equilibration at 950°C of a Tmt–Ilm_{ss} assemblage synthesized at a higher temperature produces a clockwise rotation of the original steep tie-line to a flatter one, with a Ti-poorer spinel and a Ti-richer rhombohedral phase (compare dashed and continuous lines in Fig. 1). The flattening of the tie-lines with decreasing temperature reflects the exchange of $Fe^{2+} + Ti^{4+}$ for 2 Fe^{3+} between titanomagnetite and ilmenite according to reaction (1) (see Introduction).

In some cases, however, the original high-temperature run product has been slightly oxidized because it was quenched outside the furnace, in contact with air ('external quench'; see end of section 'Sub-solidus syntheses in the Fe–Ti–Mg–Al–O system'). This oxidation affects only the surface of the sample pellet (depth <100 μm; see Lattard *et al.*, 2006, fig. 3c) where it is manifested by oxy-exsolution textures in the sense of Buddington & Lindsley (1964). Such a spatially restricted oxidation (which cannot be documented by EMP analyses because of the small size of the exsolution textures) nevertheless changes the bulk oxygen content of the sample. Consequently, the re-equilibrated 950°C assemblage displays higher magnetite and hematite contents; that is, a tie-line shifted to the left in Fig. 1.

The positive slope of the tie-lines in Fig. 1 reflects the preferred partitioning of Fe^{2+} and Ti into the rhombohedral phase. At constant temperature, however, the tie-lines are not strictly parallel (Fig. 1). Instead, their slope continuously evolves with increasing Ti/(Ti + Fe) value of both Fe–Ti oxide phases, which means that the partitioning between the two phases is strongly controlled by their compositions, as already observed in previous experimental studies (e.g. Lindsley, 1962, 1963; Spencer & Lindsley, 1981; Andersen & Lindsley, 1988; Lattard *et al.*, 2005; Evans *et al.*, 2006).

Products of sub-solidus experiments in the Fe–Ti–Mg–Al–O system

The products of sub-solidus experiments in different subsystems of the Fe–Ti–Mg–Al–O system are polycrystalline, roughly equigranular aggregates with grain sizes around 10–50 μm. They consist of Tmt–Ilm_{ss} assemblages. In six samples in the Mg-free sub-system pseudobrookite is the third phase (Psb_{ss}; solid solution between the endmembers $Fe^{3+}{}_2TiO_5$ and $Fe^{2+}Ti_2O_5$). The chemical compositions of the coexisting Tmt and Ilm_{ss} are listed in Tables 3 and 4, together with the run conditions. The compositions are plotted in Fig. 2a for the Fe–Ti–Mg–O sub-system, and in Fig. 2b for Al-bearing compositions (with or without Mg).

The MgO contents of these synthetic Tmt and Ilm_{ss} range between 0·9 and 3·0 to 3·4 wt % respectively.

Downloaded from https://academic.oup.com/petrology/article/49/6/1161/1490007 by guest on 16 August 2022

Table 2: Re-equilibration experiments performed in vacuo at 950°C (experimental step 2) on samples previously synthesized at 1100–1300°C (experimental step 1) in the Fe–Ti–O system; run conditions and chemical compositions of the product phases

Bulk	Sample no.	Experimental step 1: high-T synthesis							Experimental step 2: annealing in evacuated SiO_2 glass ampoules								
Ti/(Ti + Fe)		T (°C)	ΔNNO	mean X_{usp}	1σ	mean X_{ilm}	1σ	Remarks	T (°C)	t (days)	Assemblage	n	mean X_{usp}	1σ	n	mean X_{ilm}	1σ
8·0	6F92aD	1302	3·4	0·086	(2)	0·304	(2)		950	12	Tmt + Hem_{ss}	10	0·065	(7)	10	0·318	(2)
8·0	6F92x0.15D	1303	2·8	0·161	(2)	0·419	(2)	oxy-exs	948	14	Tmt + Hem_{ss}	10	0·121	(11)	5	0·397	(18)
20·0	6F80x0.5D	1301	1·9	0·330	(5)	0·570	(4)	oxy-exs	950	14	Tmt + Hem_{ss}	5	0·258	(2)	7	0·565	(3)
28·0	6F76x0.5D	1301	1·9	0·340	(6)	0·587	(4)	oxy-exs	951	33	Tmt + Hem_{ss}	10	0·264	(3)	10	0·586	(4)
20·0	6F80x0.75D	1301	1·4	0·414	(8)	0·630	(5)	oxy-exs	951	33	Tmt + Hem_{ss}	10	0·327	(4)	10	0·635	(4)
28·0	6F72x1.5D	1302	0·8	0·551	(4)	0·724	(4)	oxy-exs	950	28	Tmt + Ilm_{ss}	10	0·385	(4)	10	0·749	(6)
28·0	6F72x2.4D	1299	0·3	0·628	(3)	0·764	(3)		950	33	Tmt + Ilm_{ss}	10	0·536	(3)	10	0·877	(3)
28·0	6F72x4.4D	1300	−0·3	0·733	(4)	0·824	(4)		951	33	Tmt + Ilm_{ss}	10	0·670	(3)	10	0·938	(4)
37·0	6F63×8D	1300	−0·7	0·810	(7)	0·875	(4)	oxy-exs	950	37	Tmt + Ilm_{ss}	5	0·569	(4)	10	0·897	(3)
43·3	6F57x18D	1301	−1·6	0·906	(4)	0·949	(5)		948	14	Tmt + Ilm_{ss}	4	0·774	(3)	10	0·963	(5)
43·3	6F57x34D	1300	−2·4	0·965	(3)	0·979	(3)		950	21	Tmt + Ilm_{ss}	5	0·881	(5)	5	0·989	(3)
37·0	6F63x34D	1300	−2·4	0·963	(3)	0·975	(3)		950	37	Tmt + Ilm_{ss}	5	0·911	(4)	5	0·991	(3)
40·0	6IT60x49D	1300	−3·0	1·008	(4)	1·005	(6)		951	33	Tmt + Ilm_{ss}	9	0·927	(4)	10	0·996	(4)
43·3	6F57x66D	1299	−3·5	1·032	(5)	1·008	(4)		950	21	Tmt + Ilm_{ss} + Fe°	5	0·971	(3)	5	1·001	(3)
37·0	6F63x66D	1299	−3·5	1·029	(5)	1·003	(5)		950	37	Tmt + Ilm_{ss} + Fe°	5	0·978	(5)	5	1·000	(5)
37·0	5F63x2.8aD	1200	−0·1	0·648	(4)	0·804	(4)		950	21	Tmt + Ilm_{ss}	10	0·468	(14)	10	0·832	(6)
27·6	F72(f)5D	1194	−0·7	0·745	(6)	0·891	(6)		950	21	Tmt + Ilm_{ss}	10	0·698	(4)	10	0·947	(7)
37·0	5F63x33.5D	1201	−2·6	0·934	(4)	0·980	(5)		950	7	Tmt + Ilm_{ss}	10	0·887	(6)	10	0·988	(4)
45·5	5F54.5Fex83.5D	1200	−4·6	1·034	(7)	1·004	(4)		950	21	Tmt + Ilm_{ss} + Fe°	10	0·966	(5)	10	0·991	(4)
20·0	3F80x0.4D	1100	1·5	0·313	(6)	0·592	(6)		950	12	Tmt + Hem_{ss}	10	0·290	(3)	10	0·608	(3)
31·0	3F69QeD	1100	0·0	0·604	(5)	0·835	(3)		950	12	Tmt + Ilm_{ss}	10	0·549	(5)	10	0·889	(4)
37·0	3F63x16.5D	1100	−2·0	0·857	(5)	0·961	(3)		950	7	Tmt + Ilm_{ss}	10	0·801	(5)	10	0·970	(4)
37·0	3F63x30D	1100	−2·6	0·894	(8)	0·975	(7)		950	14	Tmt + Ilm_{ss}	10	0·872	(4)	10	0·980	(2)
40·0	3IT60IWD	1100	−4·4	0·974	(5)	0·996	(2)		950	14	Tmt + Ilm_{ss}	10	0·947	(5)	10	0·998	(2)

ΔNNO = log fO_2 (experimental) − log fO_2 (NNO buffer). Values for NNO after O'Neill & Pownceby (1993). t, run duration; n, number of EMP analyses; for all products of step 1, $n = 10$. All 1σ values to third decimal place. oxy-exs, oxy-exsolution textures in the products of high-temperature syntheses as a result of external quench.

The Al_2O_3 contents are low in Ilm_{ss} (maximum 1·3 wt %) but vary between 1·1 and 9·6 wt % in Tmt, with the highest content at 1100°C and relatively high contents at 1300°C in coexistence with Psb_{ss} (Tables 3 and 4). Natural Ilm_{ss} in gabbros or basalts may display higher MgO contents (up to 9 wt %; Fodor & Galar, 1997), but otherwise the Mg and Al concentrations in the Fe–Ti oxides synthesized here are comparable with their natural counterparts in basic magmatic rocks (compare, for example, with values listed in the 'GEOROC' database, MPI Mainz, Germany, available at http://georoc.mpch-mainz.gwdg.de/georoc/Entry.html).

Because the runs were performed only at moderate to low oxygen fugacity conditions (0·7 ≥ ΔNNO ≥ −4·5) the coexisting Fe–Ti oxides all have compositions poor in Fe^{3+}-bearing end-members. In this compositional region, Mg preferentially enters the rhombohedral phase and the partitioning becomes more pronounced with decreasing temperature (Fig. 2a). This is in accordance with the experimental results of Pinckney & Lindsley (1976), Pownceby & Fisher-White (1999) and Evans *et al.* (2006). With increasing fO_2, the Mg/Fe^{2+} distribution between rhombohedral and spinel phase becomes more equal (Fig. 2a) and, according to Speidel (1970), reverses between magnetite and hematite-rich Fe–Ti oxides. Such an fO_2 dependence has also been observed by Evans *et al.* (2006, fig. 9a) at lower temperatures. In contrast, Al partitions into the spinel phase, especially at lower temperatures.

Downloaded from https://academic.oup.com/petrology/article/49/6/1161/1490007 by guest on 16 August 2022

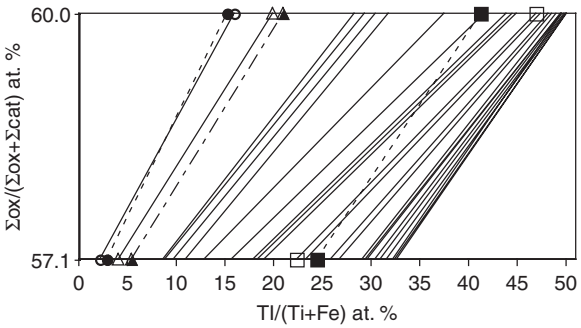

Fig. 1. Compositions [in terms of Ti/(Ti + Fe) at. %] of coexisting titanomagnetites (base) and ilmenite–hematite$_{ss}$ (top) re-equilibrated at 950°C *in vacuo* in the Fe–Ti–O system (continuous tie-lines). The two dashed lines linking black symbols show selected Tmt–Ilm$_{ss}$ pairs crystallized at 1300°C under two different fO_2 conditions. The corresponding pairs re-equilibrated at 950°C are represented by open symbols. The continuous tie-lines cross-cut the dashed ones, demonstrating that the bulk compositions did not change during the re-equilibration. The single dash–dot line defines a 1300°C tie-line that is not cross-cut by the corresponding 950°C tie-line. The latter is shifted parallel to a higher oxygen content, as a result of surface oxidation during quenching from 1300°C (see section 'Products of sub-solidus re-equilibration experiments at 950°C in the Fe–Ti–O system'). Σcat, total number of cations; Σox, total number of oxygen atoms.

The addition of Mg, however, counteracts this effect (Fig. 2b).

To better see how substituting magnesium and aluminium affect the temperature-dependent exchange equilibrium (1), we project the compositions of the Al and Mg-bearing Fe–Ti oxides onto the binaries in the simple Fe–Ti–O system, by using the same projection scheme as Evans *et al.* (2006). For Ilm$_{ss}$ the projected mole fraction of the $FeTiO_3$ endmember is calculated as $X'_{ilm} = Fe^{2+}/(Fe^{2+} + Fe^{3+}/2)$ (cation ratio). For Tmt, we assume equal partitioning of Fe^{2+} and Mg between titanate, aluminate and ferrite, which results in $X'_{usp} = Ti/(Ti + Fe^{3+}/2)$. For both Tmt and Ilm$_{ss}$ the Fe^{2+} and Fe^{3+} contents p.f.u. have been calculated by assuming stoichiometry; that is, four oxygens and three total cations for Tmt and three oxygens and two total cations for Ilm$_{ss}$ (see Tables 3 and 4). At 1200 and 1300°C, however, Tmt in equilibrium with Ilm$_{ss}$ may be cation deficient, particularly at low oxygen fugacities (e.g. Senderov *et al.*, 1993; Lattard, 1995; Lattard *et al.*, 2005). Calculated Ti^{3+} under the assumption of stoichiometry may, in fact, reflect non-stoichiometry in relation to the $Fe^{2+}_{-2}Ti^{4+}_{1}\square_{1}$ substitution. In such cases, our projection schemes are no longer adequate and no X'_{ilm} and X'_{usp} values are listed for the corresponding compositions in Tables 3 and 4.

As can be seen in the Roozeboom diagram of Fig. 3b, the projected compositions fit well within our dataset in the Fe–Ti–O system. They plot on or very near the isotherms defined by the simple system data. In particular, the Mg- and Al-bearing compositions from the 1100°C run products are in excellent agreement with those from the simple system, even in case of Al-rich Tmt. At 1200 and 1300°C the results scatter slightly more, but not as much as those in the Fe–Ti–O system of Andersen & Lindsley (1988).

Products of crystallization experiments from a basic liquid

The conditions and results of four crystallization experiments from the basic starting glass SC47-P are summarized in Table 5. The run products consist of mostly euhedral crystals embedded in glass (quenched melt phase). All samples contain Tmt, Ilm$_{ss}$ and clinopyroxene, three of them plagioclase and two a few rounded crystals of olivine. Except for the run product devoid of plagioclase (apparently plagioclase did not nucleate during this run), our observations fully confirm those of Toplis & Carroll (1995) on the products of similar experiments. Plagioclase and olivine are the first phases that crystallize on the liquidus, followed at lower temperatures by clinopyroxene and Fe–Ti oxides. Plagioclase remains a liquidus phase down to 1050°C whereas olivine begins to resorb when the temperature falls below about 1100°C (Toplis & Carroll, 1995). Indeed, resorption is indicated by the rounded form of the rare olivine crystals in our run products, in contrast to the euhedral plagioclase and clinopyroxene crystals. Crystals of the Fe–Ti oxide phases are either embedded in glass or enclosed in plagioclase or clinopyroxene crystals. Titanomagnetite forms cubic–octahedral crystals, 5–40 μm in cross-section, but many of them have hollow cores. Ilmenite$_{ss}$ forms long needles or strings of small rounded crystals, with a maximum width of about 10 μm. Because Fe–Ti oxides are abundant in all samples, there are enough crystals of desirable size for EMP analyses. There is, however, a clear correlation between the size of the crystals and the analysis totals after assignment of Fe to Fe^{2+} and Fe^{3+} based on ideal stoichiometry. Tmt with crystal sizes in the range 7–15 μm have totals between 96 and 99 wt %, whereas in the case of larger crystals the totals approach 100 wt %. Consistent with their small size, the analytical totals for the Ilm$_{ss}$ crystals are generally around 98 wt %. As discussed by Evans *et al.* (2006), the low analysis totals can be attributed to 'the minor loss of Fe and Ti counts that would have been fluorescence-induced by the continuum in larger crystals at distances from the electron-beam impact point greater than about 5 μm'. However, the cation proportions and the X'_{ilm} and X'_{usp} values are independent of the analytical totals.

Whereas plagioclase and clinopyroxene are conspicuously zoned, the Fe–Ti oxide phases do not show any apparent zoning in BSE images. Indeed, the 1σ values for the projected X'_{usp} do not exceed 0·014 (3% relative), those for X'_{ilm} are a maximum of 0·009 (1% relative; see Table 5). This means that these phases are essentially homogeneous within the single crystals and over the whole samples.

Downloaded from https://academic.oup.com/petrology/article/49/6/1161/1490007 by guest on 16 August 2022

Table 3: Chemical compositions of coexisting Tmt and Ilm_{ss} in products of sub-solidus runs at 1300°C in different subsystems of the Fe–Ti–Al–Mg–O system

System:	Fe-Ti-Al-O				Fe-Ti-Al-O with pseudobrookite						Fe-Ti-Al-Mg-O			
Sample no.:	6F70A2 x1.5	6IT60A2 x28	6IT60A2 x55	6IT60A2 x66	6IT60A2 x1.5a	6IT60A2 x6a	6F59.5A5.5 x18	6F59.5A5.5 x34	6F59.5A5.5 x34a	6F59.5A5.5 x66	6IT70M1A1 x1.5	6IT70M1A1 x6a	6IT60M1A1 x6a	6IT60M1A1 x66
T (°C)	1299·5	1300	1300	1300	1300	1299	1301	1300	1301	1299	1299·5	1299	1299	1300
t (h)	53	48	46	53	53	<61	24	>28	22	18	53	<61	<61	53
CO%	1·5	28·0	55·0	66·0	1·5	6·0	18·0	34·0	34·0	66·0	1·5	6·0	6·0	66·0
log fO_2	−5·97	−8·81	−9·79	−10·19	−5·96	−7·23	−8·32	−9·07	−9·07	−10·23	−5·97	−7·23	−7·23	−10·19
ΔNNO	0·72	−2·13	−3·10	−3·50	0·73	−0·53	−1·64	−2·39	−2·39	−3·53	0·72	−0·53	−0·53	−3·50
Tmt														
$TiO_{2\,tot}$ (wt %)*	18·95 (17)	32·03 (30)	34·54 (28)	35·37 (21)	18·85 (17)	26·27 (16)	29·85 (29)	31·63 (17)	32·09 (9)	33·75 (11)	19·89 (10)	27·38 (14)	27·28 (13)	36·26 (16)
Al_2O_3	3·42 (4)	3·01 (4)	2·75 (4)	2·74 (3)	3·82 (4)	3·98 (4)	5·43 (24)	5·85 (5)	5·95 (5)	6·51 (9)	1·51 (3)	1·13 (4)	1·97 (4)	1·31 (2)
FeO_{tot}	74·69 (30)	63·43 (35)	61·57 (20)	62·32 (33)	74·13 (35)	67·69 (30)	63·27 (23)	61·55 (34)	61·63 (26)	59·40 (34)	74·65 (31)	68·45 (34)	67·51 (33)	61·97 (26)
MgO											1·12 (3)	1·04 (2)	1·09 (2)	0·97 (2)
Ti^{4+} (p.f.u.)	0·53	0·90	0·91	0·91	0·53	0·73	0·82	0·87	0·87	0·80	0·56	0·77	0·76	0·95
Ti^{3+}	0·00	0·00	0·05	0·07	0·00	0·00	0·00	0·00	0·01	0·12	0·00	0·00	0·00	0·05
Al^{3+}	0·15	0·13	0·12	0·12	0·17	0·17	0·23	0·25	0·25	0·28	0·07	0·05	0·09	0·06
Fe^{3+}	0·79	0·08	0·00	0·00	0·78	0·36	0·12	0·01	0·00	0·00	0·82	0·42	0·39	0·00
Fe^{2+}	1·30	1·90	1·91	1·91	1·53	1·73	1·82	1·87	1·87	1·80	1·49	1·71	1·70	1·89
Mg^{2+}											0·06	0·06	0·06	0·05
X'_{usp}	0·572 (4)	0·959 (8)	—	—	0·575 (5)	0·801 (4)	0·933 (4)	0·994 (4)	0·999 (1)	—	0·574 (3)	0·785 (5)	0·783 (3)	—
Ilm_{ss}														
$TiO_{2\,tot}$ (wt %)*	38·18 (17)	50·51 (33)	52·19 (33)	52·76 (14)	38·02 (25)	44·76 (24)	49·56 (12)	51·14 (24)	51·59 (22)	52·96 (19)	38·59 (22)	44·91 (41)	45·11 (18)	53·18 (19)
Al_2O_3	1·13 (3)	0·59 (2)	0·49 (2)	0·59 (2)	1·28 (2)	1·25 (2)	1·17 (3)	1·08 (3)	1·24 (2)	1·22 (1)	0·52 (2)	0·39 (3)	0·64 (2)	0·27 (1)
FeO_{tot}	58·04 (40)	47·70 (22)	46·32 (19)	46·90 (42)	57·38 (34)	52·07 (30)	48·15 (27)	47·08 (31)	47·19 (20)	45·54 (14)	57·43 (33)	51·81 (34)	51·16 (20)	45·63 (34)
MgO											0·92 (2)	0·89 (2)	0·94 (2)	1·06 (3)
Ti^{4+} (p.f.u.)	0·73	0·97	0·99	0·99	0·73	0·86	0·94	0·97	0·97	0·96	0·73	0·86	0·86	0·99
Ti^{3+}	0·00	0·00	0·01	0·01	0·00	0·00	0·00	0·00	0·00	0·04	0·00	0·00	0·00	0·01
Al^{3+}	0·03	0·02	0·01	0·02	0·04	0·04	0·04	0·03	0·04	0·04	0·02	0·01	0·02	0·01
Fe^{3+}	0·50	0·05	0·00	0·00	0·50	0·25	0·08	0·02	0·02	0·00	0·52	0·28	0·26	0·00
Fe^{2+}	0·73	0·97	0·99	0·98	0·73	0·86	0·94	0·97	0·97	0·96	0·70	0·82	0·82	0·95
Mg^{2+}	0·00	0·00	0·00	0·00	0·00	0·00	0·00	0·00	0·00	0·00	0·03	0·03	0·04	0·04
X'_{ilm}	0·743 (4)	0·976 (4)	—	—	0·747 (4)	0·872 (4)	0·961 (4)	0·988 (3)	0·991 (4)	—	0·731 (4)	0·856 (6)	0·864 (2)	—

(continued)

Downloaded from JOURNAL OF PETROLOGY Volume 49 Number 6 June 2008 by guest on 16 August 2022

Table 3: Continued

System:	Fe–Ti–Mg–O								
Sample no.:	6F70M2x1.5	6IT60M2x6a	6F57.4M10x8	6F57.4M10x18	6F57.4M10x34	6F57.4M10x34a	6IT60M2x55	6IT60M2x66	6F57.4M10x66
T (°C)	1299·5	1299	1300	1300·5	1300	1301	1300	1300	1299
t (h)	53	<61	44	24	>28	22	46	53	18
CO%	1·5	6·0	8·0	18·0	34	34	55	66	66
log fO_2	−5·97	−7·23	−7·38	−8·32	−9·07	−9·07	−9·79	−10·19	−10·23
ΔNNO	0·72	−0·53	−0·69	−1·64	−2·38	−2·39	−3·10	−3·50	−3·53
Tmt									
$TiO_{2\,tot}$ (wt %)*	20·83 (12)	28·46 (19)	29·84 (12)	32·75 (21)	34·80 (9)	35·02 (13)	36·05 (20)	37·02 (12)	37·14 (11)
FeO_{tot}	73·87 (26)	67·47 (29)	64·71 (27)	63·45 (19)	61·27 (29)	61·12 (35)	61·03 (51)	61·25 (26)	59·34 (21)
MgO	2·17 (3)	2·08 (4)	3·08 (4)	2·94 (4)	3·00 (5)	2·97 (4)	1·95 (3)	1·94 (2)	2·99 (4)
Ti^{4+} (p.f.u)	0·58	0·79	0·83	0·90	0·96	0·96	1·00	0·98	0·98
Ti^{3+}	0·00	0·00	0·00	0·00	0·00	0·00	0·01	0·04	0·04
Fe^{3+}	0·83	0·41	0·34	0·20	0·08	0·07	0·00	0·00	0·00
Fe^{2+}	1·43	1·68	1·66	1·74	1·80	1·80	1·89	1·87	1·82
Mg^{2+}	0·12	0·12	0·17	0·16	0·16	0·16	0·11	0·11	0·16
X'_{usp}	0·583 (3)	0·794 (5)	0·830 (4)	0·900 (5)	0·96 (3)	0·97 (5)	—	—	—
Ilm_{ss}									
$TiO_{2\,tot}$ (wt %)*	39·07 (19)	46·40 (18)	49·04 (25)	51·64 (34)	52·92 (17)	53·46 (23)	53·11 (19)	53·67 (18)	54·30 (25)
FeO_{tot}	56·24 (26)	49·77 (31)	46·29 (26)	44·72 (32)	43·22 (24)	43·00 (29)	43·71 (36)	44·15 (24)	42·05 (20)
MgO	1·83 (3)	2·00 (3)	3·21 (5)	3·24 (5)	3·33 (3)	3·26 (5)	2·17 (4)	2·19 (3)	3·34 (5)
Ti^{4+} (p.f.u.)	0·74	0·88	0·92	0·96	0·98	0·99	1·00	1·00	0·99
Ti^{3+}	0·00	0·00	0·00	0·00	0·00	0·00	0·00	0·01	0·02
Fe^{3+}	0·51	0·24	0·16	0·08	0·03	0·02	0·00	0·00	0·00
Fe^{2+}	0·67	0·80	0·80	0·84	0·86	0·87	0·92	0·92	0·87
Mg^{2+}	0·07	0·07	0·12	0·12	0·12	0·12	0·08	0·08	0·12
X'_{ilm}	0·723 (4)	0·868 (5)	0·907 (4)	0·952 (5)	0·98 (4)	0·99 (4)	1·00 (1)	—	—

CO%, volume% of CO in the CO–CO_2 gas mixture; log fO_2 is derived from e.m.f. measurements with a zirconia cell. ΔNNO = log fO_2 (experimental) − log fO_2 (NNO buffer); NNO values after O'Neill & Pownceby (1993). $X'_{usp} = Ti^{4+}/(Ti^{4+} + Fe^{3+}/2)$; $X'_{ilm} = Fe^{2+}/(Fe^{2+} + Fe^{3+}/2)$.
*Values are means over 10 single EMP analyses and (1σ). For 1σ only the last digits are given.

Downloaded from https://academic.oup.com/... on 16 August 2022

Table 4: Chemical compositions of coexisting Tmt and Ilm_{ss} in products of sub-solidus runs at 1200 and 1100°C

System:	Fe–Ti–Al–O				Fe–Ti–Mg–O								
Sample no.:	5IT60A2 x5.5a	5IT60A2 x66	3F59.5A5.5 x16.5	3IT60A2 IW	5F70M2 x1.25a	5IT60M2 x5.5a	5F57.4M10 x33.5	5F57.4M10 x61.5	5IT60M2 x66	5F57.4M10 x83.5	3F57.4M10 x1.25	3F57.4M10 x16.5	3IT60M2 IW
T (°C)	1200	1200	1100	1100	1200	1200	1201	1200	1200	1200	1101	1100	1100
t (h)	>75	71	135	332	>100	>75	52	47·5	71	27	144	135	332
CO%/buffer	5·5	66·0	16·5	IW	1·3	5·5	33·5	61·5	66·0	83·5	1·25	16·5	IW
log fO_2	−8·50	−11·50	−10·90	−13·29	−7·10	−8·49	−10·33	−11·34	−11·47	−12·33	−8·44	−10·90	−13·29
ΔNNO	−0·76	−3·73	−1·96	−4·35	0·64	−0·76	−2·61	−3·61	−3·73	−4·60	0·49	−1·96	−4·35
Tmt													
$TiO_{2\,tot}$ (wt %)*	25·83 (13)	34·25 (19)	26·17 (16)	33·13 (21)	20·37 (12)	27·75 (12)	33·97 (13)	35·84 (10)	35·87 (11)	37·68 (7)	21·19 (16)	31·24 (30)	35·37 (18)
Al_2O_3	4·55 (3)	2·92 (3)	9·61 (3)	3·19 (28)									
FeO_{tot}	67·95 (27)	62·25 (27)	63·82 (36)	63·77 (37)	74·47 (46)	68·22 (27)	62·27 (16)	60·99 (33)	61·85 (24)	59·50 (24)	73·17 (29)	64·95 (29)	61·99 (30)
MgO					2·14 (3)	1·83 (2)	2·90 (4)	2·86 (4)	1·92 (3)	2·94 (4)	2·63 (3)	2·70 (3)	1·87 (4)
Ti^{4+} (p.f.u.)	0·71	0·92	0·70	0·91	0·57	0·77	0·94	0·98	0·99	0·97	0·59	0·86	0·98
Ti^{3+}	0·00	0·03	0·00	0·00	0·00	0·00	0·00	0·00	0·00	0·06	0·00	0·00	0·00
Al^{3+}	0·20	0·13	0·40	0·14									
Fe^{3+}	0·37	0·00	0·20	0·04	0·86	0·45	0·13	0·03	0·02	0·00	0·82	0·27	0·04
Fe^{2+}	1·71	1·92	1·70	1·91	1·45	1·67	1·78	1·83	1·89	1·81	1·44	1·71	1·88
Mg^{2+}					0·12	0·10	0·16	0·16	0·11	0·16	0·12	0·15	0·10
X'_{usp}	0·792 (5)	—	0·876 (6)	0·979 (4)	0·569 (4)	0·773 (6)	0·935 (3)	0·983 (4)	0·992 (4)	—	0·590 (4)	0·861 (8)	0·982 (5)
Ilm_{ss}													
$TiO_{2\,tot}$ (wt %)*	47·45 (15)	52·44 (35)	50·70 (21)	52·34 (25)	39·07 (21)	48·84 (25)	53·20 (64)	54·01 (23)	53·35 (23)	54·83 (7)	45·66 (19)	52·45 (18)	53·65 (23)
Al_2O_3	0·75 (1)	0·28 (1)	0·58 (3)	0·13 (2)									
FeO_{tot}	50·78 (27)	47·01 (26)	48·22 (34)	47·63 (20)	56·17 (27)	48·00 (18)	42·99 (37)	42·72 (39)	44·06 (38)	41·96 (21)	49·53 (21)	43·70 (23)	43·83 (18)
MgO					1·85 (3)	2·12 (4)	3·38 (15)	3·35 (3)	2·26 (3)	3·41 (4)	3·17 (3)	3·39 (5)	2·27 (2)
Ti^{4+} (p.f.u.)	0·90	0·99	0·96	0·99	0·74	0·92	0·99	1·00	1·00	0·99	0·85	0·97	1·00
Ti^{3+}	0·00	0·01	0·00	0·00	0·00	0·00	0·00	0·00	0·00	0·03	0·00	0·00	0·01
Al^{3+}	0·02	0·01	0·02	0·00									
Fe^{3+}	0·17	0·00	0·06	0·01	0·51	0·16	0·02	0·01	0·00	0·00	0·29	0·05	0·00
Fe^{2+}	0·90	0·99	0·96	0·99	0·67	0·84	0·86	0·87	0·91	0·86	0·74	0·80	0·91
Mg^{2+}					0·07	0·08	0·12	0·12	0·08	0·13	0·12	0·12	0·08
X'_{ilm}	0·913 (3)	0·999 (2)	0·972 (4)	0·994 (2)	0·723 (4)	0·911 (4)	0·986 (3)	0·997 (4)	—	—	0·834 (4)	0·970 (3)	—

(continued)

Downloaded from JOURNAL OF PETROLOGY Volume 49 Number 6 by guest on 16 August 2022

Table 4: Continued

System:	Fe–Ti–Al–Mg–O					
Sample no.:	5IT70M1A1 x1.25a	5IT70M1A1 x5.5a	5IT60M1A1 x5.5a	5IT60M1A1 x66	3IT60M1A1 WM	3IT60M1A1 IW
T (°C)	1200	1200	1200	1200	1100	1100
t (h)	>100	>75	>75	71	330	330
CO%/buffer	1·3	5·5	5·5	66·0	WM	IW
log fO_2	−7·10	−8·49	−8·49	−11·47	−10·94	−13·29
ΔNNO	0·64	−0·76	−0·76	−3·73	−2·01	−4·35
Tmt						
$TiO_{2\,tot}$ (wt %)*	19·34 (13)	26·99 (18)	26·59 (16)	35·34 (9)	28·91 (17)	34·35 (14)
Al_2O_3	1·22 (4)	1·12 (3)	1·37 (3)	1·29 (8)	1·61 (10)	1·29 (5)
FeO_{tot}	75·10 (38)	68·77 (33)	68·81 (29)	62·19 (38)	67·15 (40)	63·00 (27)
MgO	1·09 (3)	0·99 (3)	0·91 (2)	0·94 (2)	0·86 (3)	0·89 (4)
Ti^{4+} (p.f.u.)	0·54	0·76	0·75	0·97	0·80	0·95
Ti^{3+}	0·00	0·00	0·00	0·01	0·00	0·00
Al^{3+}	0·05	0·05	0·06	0·06	0·07	0·06
Fe^{3+}	0·86	0·44	0·45	0·00	0·32	0·04
Fe^{2+}	1·48	1·70	1·69	1·91	1·76	1·90
Mg^{2+}	0·06	0·05	0·05	0·05	0·05	0·05
X'_{usp}	0·558 (4)	0·774 (5)	0·768 (5)	—	0·834 (5)	0·98 (5)
Ilm$_{ss}$						
$TiO_{2\,tot}$ (wt %)*	38·34 (14)	47·72 (29)	47·49 (23)	53·04 (19)	51·02 (29)	52·79 (24)
Al_2O_3	0·30 (2)	0·13 (2)	0·17 (2)	0·07 (2)	0·05 (2)	0·00
FeO_{tot}	57·33 (30)	49·45 (38)	49·84 (29)	45·41 (26)	47·05 (36)	45·63 (34)
MgO	0·91 (2)	1·14 (3)	1·03 (3)	1·10 (3)	1·08 (2)	1·07 (6)
Ti^{4+} (p.f.u.)	0·73	0·91	0·90	1·00	0·97	1·00
Ti^{3+}	0·00	0·00	0·00	0·01	0·00	0·00
Al^{3+}	0·01	0·00	0·00	0·00	0·00	0·00
Fe^{3+}	0·52	0·18	0·19	0·00	0·07	0·00
Fe^{2+}	0·70	0·86	0·86	0·95	0·93	0·96
Mg^{2+}	0·03	0·04	0·04	0·04	0·04	0·04
X'_{ilm}	0·729 (3)	0·905 (6)	0·901 (4)	—	0·966 (3)	0·998 (3)

CO%/buffer is volume% of CO in the CO–CO_2 gas mixture or buffer enclosed together with the sample in a SiO_2 glass ampoule. Buffer: IW, Fe–wustite; WM, wustite–magnetite. Oxygen fugacity values after O'Neill & Pownceby (1993) or O'Neill (1988). log fO_2 is derived from e.m.f. measurements with a zirconia cell. ΔNNO = log fO_2 (experimental) – log fO_2 (NNO buffer). NNO values after O'Neill & Pownceby (1993). $X'_{usp} = Ti^{4+}/(Ti^{4+} + Fe^{3+}/2)$; $X'_{ilm} = Fe^{2+}/(Fe^{2+} + Fe^{3+}/2)$. *Values are means over 10 single EMP analyses and (1σ) to the last decimal place.

Downloaded from https://academic.oup.com/petrology/article/37/5/1165/1485016 by guest on 16 August 2022

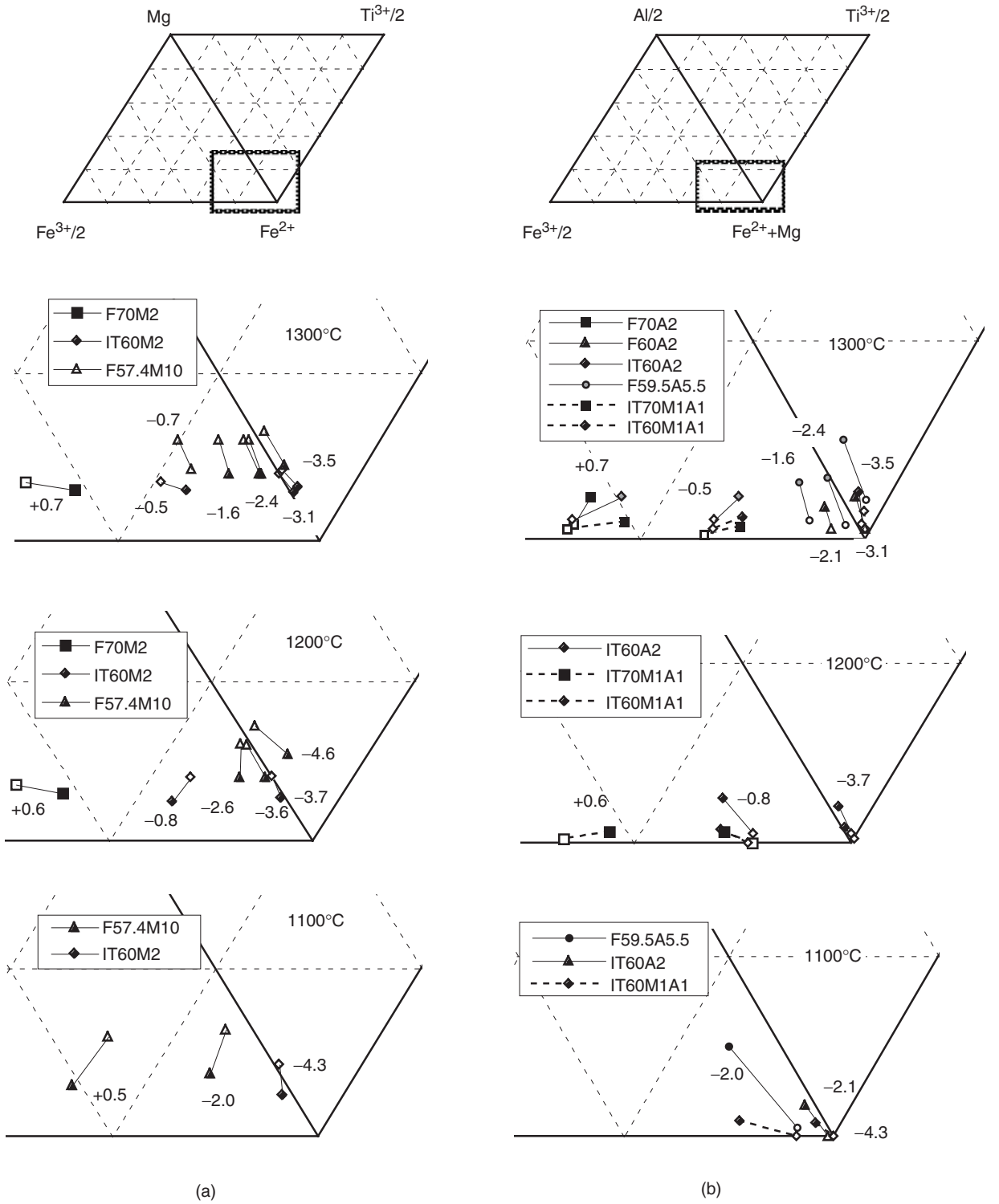

Fig. 2. Compositions of coexisting Ilm_{ss} (open symbols) and Tmt (filled symbols) from run products in the Fe–Ti–Mg–O system (a) and in the Fe–Ti–Al–Mg–O system (b) at 1300, 1200 and 1100°C. Symbols indicate the starting materials. In (b) dashed tie-lines are for Mg-bearing compositions; continuous tie-lines for Mg-free compositions. Gray symbols refer to Tmt in coexistence with Ilm_{ss} + Psb_{ss} (1300°C, Fe–Ti–Al–O system). Numbers indicate the ΔNNO values.

Downloaded from https://academic.oup.com/petrology/article/49/6/1161/1490007 by guest on 16 August 2022

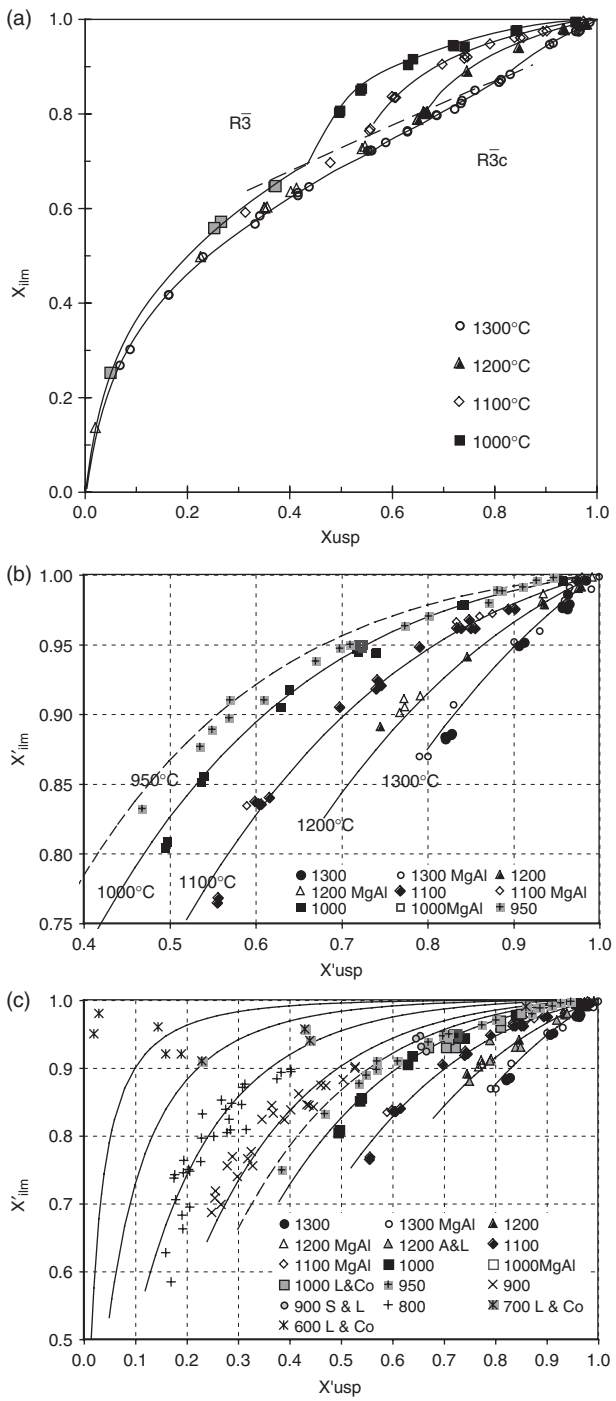

Fig. 3. Roozeboom diagram X'_{ilm} vs X'_{usp} with values for coexisting synthetic Tmt and Ilm_{ss} (symbols) and isotherms (curves). (a) Data points from run products in the Fe–Ti–O system [1000–1300°C data from Lattard *et al.* (2005); 950°C data from section 'Products of sub-solidus re-equilibration experiments at 950°C in the Fe–Ti–O system'], hand-drawn isotherms and dashed line marking the phase transition between the $R\bar{3}$ and the $R\bar{3}c$ space groups in the rhombohedral oxide (after Harrison *et al.*, 2000). In the lower left part of the diagram only the 1000 and the 1300°C isotherms are drawn. (b) Part of the Roozeboom diagram relevant to Ilm_{ss} with the $R\bar{3}$ space group. Data points from the products of runs at 950–1300°C in the Fe–Ti–O system (filled symbols) and in the Fe–Ti–Mg–Al–O system (open symbols), as discussed in the text and by Lattard *et al.* (2005). Isotherms calculated as in sub-section 'Thermometry'. (c) Same data points as in (b) complemented with results from the literature and calculated isotherms for 600–900°C. Abbreviations: 1200 A & L, Andersen & Lindsley (1988); 1000 L & Co, Lindsley (1962, 1963), Spencer & Lindsley (1981) and Andersen & Lindsley (1988); 900 S & L, Spencer & Lindsley (1981); 700 L & Co and 600 L & Co, Lindsley (1962, 1963) and Spencer & Lindsley (1981). Other abbreviations refer to the data displayed in (b).

As in the sub-solidus samples (preceding section), the Al partitioning between the Fe–Ti oxide phases is in favour of Tmt, whereas Mg prefers Ilm_{ss}. However, in contrast to the sub-solidus samples, the Al and Mg contents of the Fe–Ti oxide phases are significantly higher. As will be shown later, these higher Mg and Al contents do not disturb the Fe–Ti partitioning between Tmt and Ilm_{ss}. The projected X'_{ilm}–X'_{usp} pairs are in good agreement with values for the Mg- and Al-free system. They will be used to test our numerical version of the Tmt–Ilm_{ss} thermo-oxybarometer.

NUMERICAL FITS TO EXPERIMENTAL DATA

We have performed numerical fits to the experimental results presented in the preceding sections, together with other published datasets, with the aim of deriving simple equations to estimate temperature and oxygen fugacity from the compositions of coexisting Tmt and Ilm_{ss} for a restricted T–fO_2 realm. We take advantage of the fact that in our run products in the Fe–Ti–Al–Mg–O system, the projected compositions of the Fe–Ti oxides are in good agreement with those in the simple Fe–Ti–O system. Because this is also the case for the major part of the data of Evans *et al.* (2006), we shall also include these results in our dataset.

Thermometry

The Roozeboom diagram of X'_{ilm} vs X'_{usp} (Fig. 3) is a very convenient basis for the numerical calibration of the Tmt–Ilm_{ss} thermometer based on an experimental dataset. The core of this dataset is the group of results in the Fe–Ti–O system that includes literature data (Lindsley, 1962, 1963; Spencer & Lindsley, 1981; Andersen & Lindsley, 1988; Senderov *et al.*, 1993), our recently published results (Lattard *et al.*, 2005) and the 950°C results presented in Table 2. The dataset also comprises the results of Evans *et al.* (2006) in the Fe–Ti–Al–Mg–Mn–O system, and the data listed in Tables 3 and 4, which were all projected into the simple system with the schemes described previously. Results from a few older experimental studies (in particular, Webster & Bright, 1961; Taylor, 1964; Speidel, 1970) were not included because the corresponding phase compositions are uncertain.

Downloaded from https://academic.oup.com/petrology/article/49/6/1161/1490007 by guest on 16 August 2022

Table 5: Chemical compositions of Fe–Ti oxide phases from crystallization experiments on composition SC47-P

Run no.	2SC47x1.25	2SC47x4	2.5SC47x4.5	2SC47x6
Run history				
T initial (°C)	1140	1140	1150	1140
D initial (h)	10	10	8	10
Ramp (°C/h)	3	3	3	3
D ramp (h)	29	29	23	29
T final (°C)	1053	1052	1082	1053
D final (h)	150	50	60	246
CO%	1·25	4	4·5	6·3
log fO_2	−9·40	−10·20	−10·00	−10·51
ΔNNO final	0·16	−0·62	−0·83	−0·95
Run products	Gl, Pl, Cpx, Tmt, Ilm_{ss}	Gl, (Ol), Cpx, Tmt, Ilm_{ss}	Gl, Pl, (Ol), Cpx Tmt, Ilm_{ss}	Gl, Pl, Cpx, Tmt, Ilm_{ss}
Tmt				
n	49	21	37	31
TiO_2 (wt %)	17·53 (50)	22·98 (56)	23·81 (23)	24·68 (26)
Al_2O_3	1·59 (6)	3·27 (7)	2·15 (5)	1·62 (4)
FeO_{tot}	73·90 (59)	67·28 (80)	66·22 (59)	66·86 (68)
MgO	2·28 (7)	2·61 (7)	2·97 (7)	1·9 (4)
Ti^{4+} (p.f.u.)	0·493	0·638	0·669	0·703
Al^{3+}	0·070	0·142	0·095	0·720
Fe^{3+}	0·944	0·582	0·566	0·522
Fe^{2+}	1·366	1·495	1·504	1·596
Mg^{2+}	0·127	0·143	0·166	0·107
X'_{usp}	0·511 (14)	0·687 (17)	0·703 (7)	0·729 (6)
Ilm_{ss}				
n	19	11	44	9
TiO_2 (wt %)	42·36 (39)	48·72 (33)	49·27 (32)	48·28 (28)
Al_2O_3	0·10 (3)	0·15 (4)	0·05 (2)	0·00
FeO_{tot}	51·14 (66)	45·06 (52)	44·12 (43)	44·82 (59)
MgO	2·68 (9)	3·21 (7)	3·70 (8)	2·82 (4)
Ti^{4+} (p.f.u.)	0·809	0·924	0·932	0·938
Al^{3+}	0·003	0·004	0·001	0·000
Fe^{3+}	0·379	0·147	0·135	0·124
Fe^{2+}	0·708	0·804	0·793	0·845
Mg^{2+}	0·101	0·121	0·139	0·930
X'_{Ilm}	0·789 (9)	0·916 (9)	0·922 (5)	0·932 (6)

T initial, initial run temperature above the liquidus; *D* initial, duration at initial run temperature; *D* ramp, duration of ramp between initial and final run temperature; *T* final, final, sub-liquidus run temperature; *D* final, duration at final run temperature; CO%, volume % of CO in the CO–CO_2 gas mixture; log fO_2 is derived from e.m.f. measurement with a zirconia cell at final temperature; ΔNNO = log fO_2 (experimental) − log fO_2 (NNO buffer); values for NNO after O'Neill & Pownceby (1993). Gl, glass; Pl, plagioclase; Ol, olivine; Cpx, clinopyroxene; Tmt, titanomagnetite; Ilm_{ss}, ilmenite–$hematite_{ss}$. Parentheses indicate very low modal proportions. *n*, number of single analyses; values given are means and (1σ). $X'_{usp} = Ti/(Ti + Fe^{3+}/2)$; $X'_{ilm} = Fe^{2+}/(Fe^{2+}+Fe^{3+}/2)$.

As can be seen from Fig. 3, we have plotted only those Tmt–Ilm_{ss} pairs that involve Ilm_{ss} with the long-range ordered ilmenite structure (space group $R\bar{3}$). Following Harrison *et al.* (2000), the corresponding compositional fields are restricted to $X_{ilm} > 0{\cdot}875$ at 1300°C, but gradually widen with decreasing temperatures (e.g. $X_{ilm} > 0{\cdot}575$ at 800°C). There are several reasons for limiting our dataset to those Tmt–Ilm_{ss} pairs. The first is that the spacing of the isotherms is reasonably wide only on the '$R\bar{3}$ side' of the Roozeboom diagram (Fig. 3a). We see no chance to provide an acceptable numerical fit for the part of the Roozeboom diagram that involves Ilm_{ss} richer in the Fe_2O_3 endmember (disordered structure with space group $R\bar{3}$c), because the corresponding isotherms are too narrowly spaced (Fig. 3a). Moreover, our experimental results on Mg- and Al-bearing compositions essentially concern Ilm_{ss} rich in the $FeTiO_3$ endmember and they provide very little information on the effect of minor components on hematite-rich compositions. The results of Evans *et al.* (2006) show that at 800 and 900°C the isotherms are not very sensitive to minor components on the '$R\bar{3}$ side' but strongly influenced by them on the '$R\bar{3}$c side'. This would probably also hold for higher equilibration temperatures. On the whole, we shall restrict our numerical fits to the compositional realm indicated in Fig. 3c, with the aim of specifically addressing Fe–Ti oxide parageneses in basic and intermediate magmatic rocks that typically include Ti-rich Ilm_{ss} and Tmt of intermediate compositions.

Our first idea was to fit, through least-squares methods, $X'_{ilm} = f(X'_{usp}, T)$ to a second- or third-order polynomial function, with the condition that $X'_{ilm} = 1$ for $X'_{usp} = 1$. However, we could not retrieve a satisfying, stable solution for temperatures in the range 700–1300°C. In particular, the high X'_{ilm} and X'_{usp} values at $T \leq 1000$°C were badly reproduced. Therefore we turned to an expression derived by writing the law of mass action for reaction (1):

$$-\Delta G^*_r = RT \ln K, \text{ where } K = \frac{a_{ilm} a_{mag}}{a_{hem} a_{usp}}.$$

This equation can be rewritten as

$$\frac{a_{ilm}}{a_{hem}} = \frac{a_{usp}}{a_{mag}} \exp\left(-\frac{\Delta G^*_r}{RT}\right).$$

With the simplifications $a_{ilm} = X_{ilm}$ and $a_{hem} = X_{hem}$ we can write

$$X_{ilm} = X_{hem} \frac{a_{usp}}{a_{mag}} \exp\left(-\frac{\Delta G^*_r}{RT}\right)$$

and considering that $X_{ilm} = 1 - X_{hem}$, we obtain

$$\frac{1}{X_{hem}} = \frac{a_{usp}}{a_{mag}} \exp\left(-\frac{\Delta G^*_r}{RT}\right) + 1.$$

Downloaded from https://academic.oup.com/petrology/article/49/6/1161/1490007 by guest on 16 August 2022

We approximate $-\Delta G_r^*/RT$ through the polynomial $(K_1/T)+K_2+(K_3/T^2)$, with the constants K_1, K_2 and K_3 and arrive at the following expression:

$$X_{ilm} = 1 - \frac{1}{1/X_{\rm hem}} = 1 - \frac{1}{\exp\left(\frac{K_1}{T}+K_2+\frac{K_3}{T^2}\right)\frac{a_{\rm usp}}{a_{\rm mag}}+1}. \quad (3)$$

The activities of the ulvöspinel and magnetite components in the spinel phase are $a_{\rm usp}=X_{\rm usp}\ \gamma_{\rm usp}$ and $a_{\rm mag}=X_{\rm mag}\ \gamma_{\rm mag}$ and the activity coefficients, $\gamma_{\rm usp}$ and $\gamma_{\rm mag}$ are derived from expressions used for symmetrical solution models; that is,

$$RT\ \ln\ \gamma_{\rm usp} = X_{\rm usp}\ [W_{\rm Gmag} + 2X_{\rm mag}(W_{\rm Gusp} - W_{\rm Gmag})]$$

and

$$RT\ \ln\ \gamma_{\rm mag} = X_{\rm mag}\ [W_{\rm Gusp} + 2X_{\rm usp}(W_{\rm Gmag} - W_{\rm Gusp})]$$

where $W_{\rm Gusp}$ and $W_{\rm Gmag}$ are constants, and $X_{\rm usp}$, $X_{\rm mag}$ and $X_{\rm hem}$ are the mole fractions of the corresponding components in the spinel and the coexisting rhombohedral phase, respectively. To account for Fe–Ti oxides with complex compositions, we use the projected mole fractions (see preceding section), which are calculated from the following cation ratios, assuming stoichiometric compositions:

$$X'_{\rm usp} = {\rm Ti}/({\rm Ti} + {\rm Fe}^{3+}/2) \quad (4a)$$

$$X'_{\rm ilm} = {\rm Fe}^{2+}/({\rm Fe}^{2+} + {\rm Fe}^{3+}/2) \quad (4b)$$

$$X'_{\rm mag} = 1 - X'_{\rm usp} \quad (4c)$$

$$X'_{\rm hem} = 1 - X'_{\rm ilm}. \quad (4d)$$

We calculate $X_{\rm ilm}({\rm calc})$ from equation (3), $X'_{\rm ilm}({\rm meas})$ from (4b) and finally $\Delta X'_{\rm ilm} = X_{\rm ilm}({\rm calc}) - X'_{\rm ilm}({\rm meas})$. The squared $\Delta X'_{\rm ilm}$ values are added up and the sum is minimized by using a GRG2 non-linear quadratic optimization algorithm (Lasdon & Waren, 1978) to determine the K_1, K_2, K_3, $W_{\rm Gusp}$ and $W_{\rm Gmag}$ parameters.

One of the advantages of this optimization procedure is that it allows weighting of the $\Delta X'_{\rm ilm}$. Because our aim was to adequately fit the experimental data at high temperatures, we chose to weight all results gained from experiments at $T \geq 1000$°C (Lindsley, 1962, 1963; Andersen & Lindsley, 1988; Senderov *et al.*, 1993; Lattard *et al.*, 2005; present data in Tables 3 and 4) with a factor of 500. Results from experiments performed at $800 \leq T \leq 950$°C (Evans *et al.*, 2006; present data in Table 2), which scatter much more in the Roozeboom diagram (Fig. 3c), were weighted with a factor of 100; those of experiments at lower temperatures (Lindsley, 1962, 1963; Spencer & Lindsley, 1981) with a factor of 10. The low weighting of the latter data was also chosen to account for the fact that the experiments at 600–750°C were reversals that did not yield equilibrium compositions but provided compositional brackets. This is also the case for two experimental brackets at 980°C (Spencer & Lindsley, 1981). A factor of 10 was also applied to the five data points at 800°C with $X'_{\rm ilm}$ values between 0·70 and 0·58, which define a break in slope of the isotherm (Fig. 3c), possibly related to the solvus in the rhombohedral oxide series (Evans *et al.*, 2006). On the whole, we have regressed the five parameters K_1, K_2, K_3, $W_{\rm Gusp}$ and $W_{\rm Gmag}$ on the basis of 189 data points, whereby 83 $X'_{\rm ilm}$ values were weighted with a factor of 500, 69 with a factor of 100 and 37 with a factor of 10. The regressed parameters are given in Table 6.

Using these parameters one can easily calculate $X'_{\rm ilm}$ as a function of $X'_{\rm usp}$ at any given temperature and derive isotherms in the Roozeboom diagram, as depicted in Fig. 3b and c. As expected, these calculated isotherms fit the experimental data very well at temperatures in the range 1000–1300°C. They also reasonably match the experimental results at 950°C and those at 800°C, except for the values at $X'_{\rm ilm} < 0{\cdot}75$ discussed above. In contrast, the model isotherm at 900°C does not fit the experimental data points well. Its slope is somewhat too steep for $0{\cdot}8 < X'_{\rm ilm} < 0{\cdot}9$ and the curvature is not strong enough towards

Table 6: Coefficients and parameters of the expressions obtained through numerical fits

Fit for thermometry

$$X'_{\rm ilm} = f(T, X'_{\rm usp}) = 1 - \frac{1}{\exp\left(\frac{K_1}{T}+K_2+\frac{K_3}{T^2}\right)\frac{a_{\rm usp}}{a_{\rm mag}}+1}$$

with

$a_{\rm usp} = X_{\rm usp}\ \gamma_{\rm usp}$

$a_{\rm mag} = X_{\rm mag}\ \gamma_{\rm mag}$

$RT\ \ln\ \gamma_{\rm usp} = X_{\rm usp}\ [W_{\rm Gmag} + 2\ X_{\rm mag}\ (W_{\rm Gusp} - W_{\rm Gmag})]$

$RT\ \ln\ \gamma_{\rm mag} = X_{\rm mag}\ [W_{\rm Gusp} + 2\ X_{\rm usp}\ (W_{\rm Gmag} - W_{\rm Gusp})]$

$W_{\rm Gusp}$	−8872·94084	K_1	6330·46473
$W_{\rm Gmag}$	−9131·68929	K_2	−4·77394
		K_3	2205242·17573

Fit for oxybarometry

$$\Delta{\rm NNO} = \Delta{\rm NNO_{MH}} + a_1X'_{\rm usp} + a_2(X'_{\rm usp})^2 + a_3(X'_{\rm usp})^3 + b_1X'_{\rm usp}T + b_2X'_{\rm usp}T^2 + b_3X'_{\rm usp}T^3 + c_1(X'_{\rm usp})^2T + c_2(X'_{\rm usp})^2T^2 + c_3(X'_{\rm usp})^2T^3$$

with

$$\Delta{\rm NNO_{MH}} = [-501348 + 285{\cdot}4\,T + 0{\cdot}3548\ (P-1) + 478967 - 248{\cdot}514\,T + 9{\cdot}7961\,T\ \ln(T) + 0{\cdot}8764(P-1)]/\ 8{\cdot}3143\,T\ \ln(10)$$

a_1	48·45568	c_1	0·72063
a_2	−301·09335	c_2	−0·00054
a_3	−16·96296	c_3	$1{\cdot}3468 \times 10^{-7}$
b_1	−0·17458		
b_2	0·00015		
b_3	$-4{\cdot}3250 \times 10^{-8}$		

T is in Kelvin. Values for NNO buffer after O'Neill & Pownceby (1993); for MH buffer after Hemingway (1990). Volumes of solid phases after Robie *et al.* (1979).

Downloaded from https://academic.oup.com/petrology/article/49/6/1161/1490007 by guest on 16 August 2022

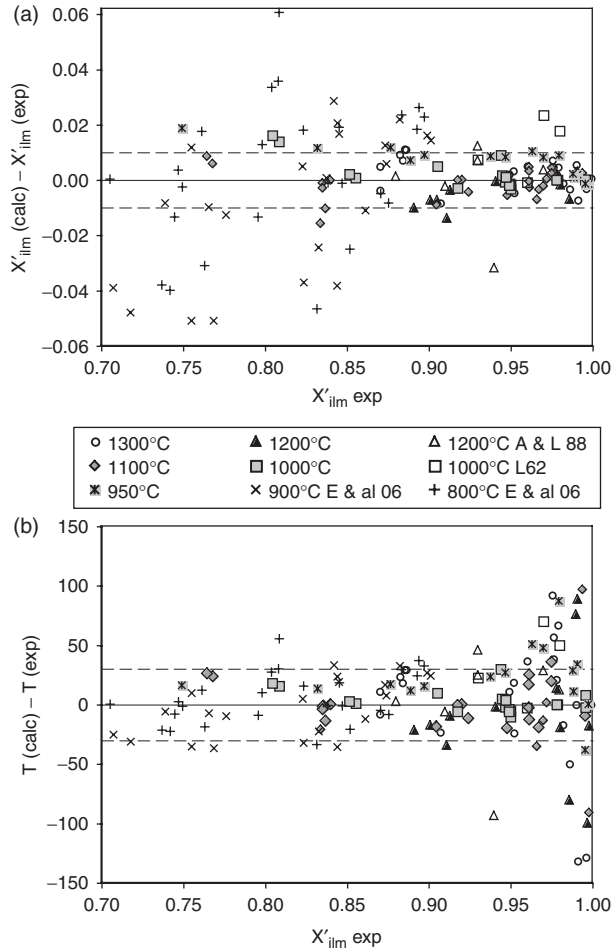

Fig. 4. Differences between experimental values and values calculated with the numerical fits presented in the sub-section 'Thermometry' as a function of the projected mole fraction of the ilmenite endmember. The data points are Tmt–Ilm_{ss} pairs used for calibration of the numerical fits. Filled symbols and asterisks on gray field: own experiments (see text and Lattard *et al.*, 2005). Crosses and open symbols: literature results at 1200°C (Δ, Andersen & Lindsley, 1988), 1000°C (□, Lindsley, 1962), 900°C (×, Evans *et al.*, 2006), 800°C (+, Evans *et al.*, 2006). (a) Differences between X'_{ilm}(calc) [i.e. X'_{iIm} calculated from expression (2)] and X'_{ilm}(exp) (i.e. those obtained from the EMP analyses of synthetic Ilm_{ss}). Dashed lines mark differences of ±0·01. (b) Differences between calculated temperatures T(calc) and temperatures set up during the experiments T(exp). Dashed lines mark differences of ±30°C.

lower X'_{ilm} and X'_{usp} (Fig. 3c). In fact, the curvature of all isotherms should ideally be slightly stronger to better account for the lowest X'_{ilm} and X'_{usp} values. Figure 4a confirms that the calculated X'_{ilm} well approximates the measured values at temperatures between 1000 and 1300°C. With very few exceptions (less than 10% of the data), the difference is less than 0·01. But at $T \leq 900$°C, where the experimental data scatter much more and the calculated isotherms do not perfectly match the experimental trends, the difference between experimental and modelled value can reach ±0·06. A close examination of the 800 and 900°C data of Evans *et al.* (2006) reveals that those with the strongest $\Delta X'_{ilm}$ all stem from very few experiments; that is, runs 13 and 26 at 900°C, and runs 9, 11 and 22 at 800°C, whereby the two last named belong to what Evans *et al.* (2006) called their 'problem' experiments. It is not clear whether these run products reached equilibrium.

For any given X'_{ilm}, X'_{usp} pair we can calculate the corresponding equilibrium temperature by iteration nesting from equation (3) (a macro is given in a Supplementary Data Excel worksheet at http://www.petrology.oxfordjournals.org/). For X'_{ilm} values up to 0·95 nearly all the calculated temperatures reproduce the experimental values within ±30°C. Even the 800 and 900°C results that show significant differences between experimental and modelled X'_{ilm} values yield calculated temperatures that are at most ±35°C from the experimental values. Only one 'problem' experiment at 800°C (run 11-IV; Evans *et al.*, 2006) and two bracketing runs at 1200°C (Andersen & Lindsley, 1988) show stronger divergences (Fig. 4b), which may reflect a lack of equilibrium in the experimental products. For X'_{ilm} values above 0·95 the discrepancies between experimental and calculated values increase considerably (Fig. 4b), which is a direct consequence of the narrow spacing of the isotherms at very high X'_{ilm} and X'_{usp} values (Fig. 3b and c). Such Ti-rich compositions are, however, of little significance for terrestrial magmatic rocks.

We have checked the effect of weighting the results from experiments performed in the temperature range 800–950°C with the same high factor (500) as for the results at 1000–1300°C. This slightly improves the calculated X'_{ilm} values for 800 and 900°C but worsens those for the higher temperature experiments. As the calculated temperatures are hardly influenced by the different weightings we have kept our original weighting factors.

Oxybarometry

The Tmt–Ilm_{ss} oxybarometer is based on iron redox equilibria [see reaction (2)] and the compositions of coexisting Tmt and Ilm_{ss} are unique at any given P–T–fO_2 condition. With increasing fO_2 both Fe–Ti oxide phases increase their Fe^{3+} contents; that is, decrease the proportions of their Ti-rich end-members. In the case of Tmt the compositional shift as a function of oxygen fugacity is small at low fO_2 values ($\Delta NNO < -2$), but becomes strong at moderate fO_2 values and decreases again at high values ($\Delta NNO > 1$). In a ΔNNO vs X'_{usp} plot this results in smooth, roughly parallel isotherms that can be fitted by a third-order polynomial function (Fig. 5). Similar behaviour might have been expected for the rhombohedral oxides; however, because of complications associated with long-range order and structural transitions, the isotherms have a complex shape and cross over (see Lattard *et al.*, 2005, fig. 8); that is, they cannot be adequately fitted with

Downloaded from https://academic.oup.com/petrology/article/49/6/1161/1490007 by guest on 16 August 2022

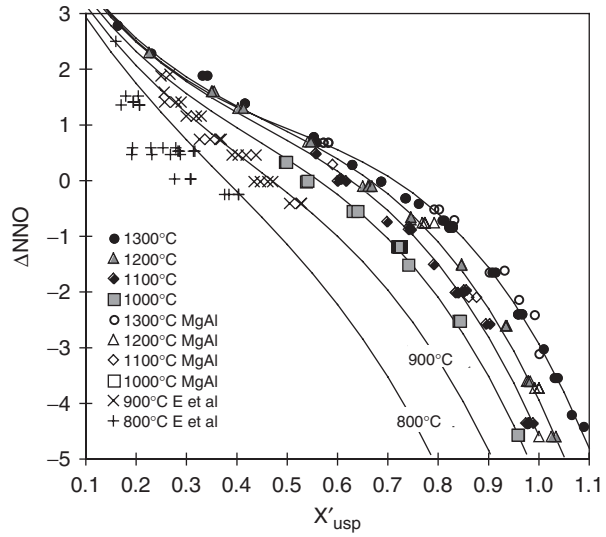

Fig. 5. Relationship between Tmt composition (in term of X'_{usp}) and oxygen fugacity (expressed as $\Delta NNO = \log fO_2$ (exp) – $\log fO_2$ (NNO buffer) for synthetic Tmt–Ilm_{ss} assemblages in the systems Fe–Ti–O (filled symbols; Lattard *et al.*, 2005), Fe–Ti–Mg–Al–O (open symbols; data from Tables 3 and 4) and Fe–Ti–Mg–Mn–Al–O (×, +; Evans *et al.*, 2006). The isotherms were obtained from the least-square fits discussed in the sub-section 'Oxybarometry'.

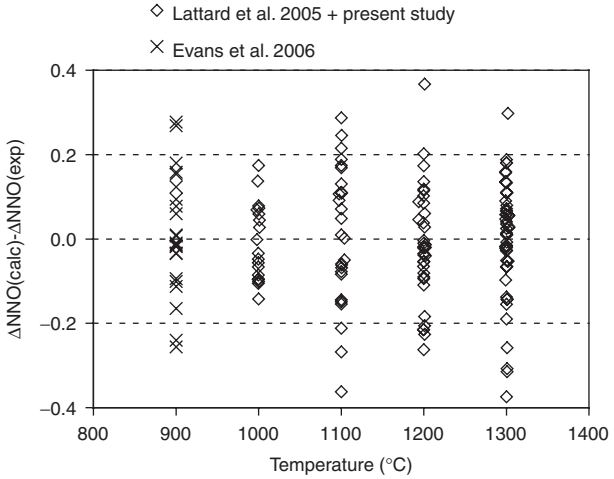

Fig. 6. Differences between calculated and experimental ΔNNO values as a function of temperature for our experimental products in the Fe–Ti–O system (Lattard *et al.*, 2005) and in the Fe–Ti–Mg–Al–O system (present study; Tables 3 and 4) and for the 900°C run products of Evans *et al.* (2006) in the Fe–Ti–Mg–Mn–Al–O system.

simple functions. Consequently, we do not use the Ilm_{ss} isotherms to derive an expression for oxybarometry.

Coming back to the effect of fO_2 on titanomagnetite, we note that the projected compositions of the Tmt synthesized at 1100–1300°C in the Fe–Ti–Mg–Al–O system plot more or less on the same isotherms as the compositions in the simple system (Fig. 5). In contrast, Evans *et al.* (2006) have shown that at $T \leq 900$°C in the Fe–Ti–Mg–Mn–Al–O system, the X'_{usp} values at any given ΔNNO are systematically shifted as a function of their compositions. As can be seen in Fig. 5, the spread in the X'_{usp} values at 900°C ranges up to 0·1 and is even stronger at 800°C. Consequently, the data at 800°C have not been used for our numerical fit.

The data used for the fit comprise the results of the present study for Mg- and/or Al-bearing Tmt under sub-solidus conditions at 1300–1100°C (Tables 3 and 4), those of Evans *et al.* (2006) at 900°C in the Fe–Ti–Al–Mg–Mn–O system, and those of Lattard *et al.* (2005) in the simple Fe–Ti–O system at 1000–1300°C. In contrast to the fitting of reaction (1), we have not restricted our database to Fe–Ti oxide pairs with Ilm_{ss} with the $R\bar{3}$ space group, which occur only at low ΔNNO values. Instead, we have considered Tmt from all available pairs to better constrain the isotherms to high ΔNNO values. We have fitted the data to a third-order polynomial function for $\Delta NNO = f(X'_{Usp}, T)$ with a standard least-squares algorithm for multiple linear regressions (RGP function of Microsoft Excel™). The ΔNNO values for $X'_{usp} = 0$ were fixed to those of the magnetite–hematite buffer using the data of Hemingway (1990). In fact, fits performed without this constraint lead to very similar results at $X'_{usp} = 0$. The coefficients of the polynomial functions are listed in Table 6.

The calculated isotherms fit the experimental data reasonably well for temperatures in the range 900–1200°C (Fig. 5). At 1300°C, however, the calculated isotherm does not perfectly reproduce the experimental data. This may result partly from the effect of cation defects, which are undoutedly abundant in the Fe–Ti–O system at low oxygen fugacity values, but may have variable concentrations at higher ΔNNO, depending on the redox state and the Al and Mg concentrations (Lattard *et al.*, 2005; Sauerzapf, 2006). The calculated 900°C isotherm yields only mean ΔNNO values, and the 800°C isotherm yields essentially maximum ΔNNO values at any given X'_{usp} (Fig. 5). As discussed by Evans *et al.* (2006), there is a systematic shift of X'_{usp} with the bulk composition of the starting material. Interestingly, the strongest discrepancy between the experimental results and our 800°C isotherm is for bulk composition I, which is in the Fe–Ti–Al–O system. The best agreement is for bulk composition IV, which includes Al, Mg and Mn and is the most relevant for natural Fe–Ti oxide assemblages.

In the temperature range 900–1300°C, 95% of the ΔNNO estimates with our fitted polynomial reproduce the experimental values within ±0·3, and 90% within ±0·2. This is a very good agreement, given that ±0·2 is the uncertainty of the e.m.f. measurements of the oxygen fugacity (Fig. 6). At 800°C or lower temperatures, however, our polynomial can yield overestimates in ΔNNO of up to 1·2 for Mg- and Mn-free compositions.

Downloaded from https://academic.oup.com/petrology/article/49/6/1161/1490007 by guest on 16 August 2022

TESTS OF THE NEW TITANOMAGNETITE–ILMENITE THERMO-OXYBAROMETER VERSION WITH INDEPENDENT EXPERIMENTAL DATA

On the basis of the numerical fits presented in the preceding sections, both temperature and oxygen fugacity can be calculated from the compositions of coexisting Tmt–Ilm_{ss} that are moderately substituted with Al, Mg and/or Mn. Our fits are based on experimental data in the temperature range 800–1300°C. Because they are not based on a rigorous thermodynamic model—in particular no solid-solution models for the Fe–Ti oxides—these fits should not be used for assemblages equilibrated at significantly lower temperatures. As shown in Fig. 5, the oxygen fugacity estimates yield only maximum values at temperatures below 900°C. It is also crucial not to use the thermometry fit for Ilm_{ss} with the long-range disordered hematite structure in the $R\bar{3}c$ space group. According to Harrison *et al.* (2000), this limits the application to compositions with $X_{ilm} > 0{\cdot}59$ at 800°C, but in excess of 0·70 at 1000°C and 0·82 at 1200°C. These values are only approximate because additional elements may shift the X'_{ilm} value for the order–disorder transition. In any case, misuse of our fits for more Fe-rich ilmenite compositions would yield significant overestimates of the equilibration temperature.

In the following section we test our numerical expressions on independent experimental results relevant to the crystallization and differentiation of basic liquids. There are numerous experimental studies in which Fe–Ti oxide phases form part of the crystalline assemblages in equilibrium with the surrounding liquid. However, we have found only a few studies in the literature that report the compositions of coexisting Tmt and Ilm_{ss} equilibrated during experiments in the desired temperature and oxygen fugacity range. These are the data of Juster *et al.* (1989), Snyder *et al.* (1993), Toplis *et al.* (1994), Gardner *et al.* (1995*b*), Toplis & Carroll (1995), Scaillet & Evans (1999) and Prouteau & Scaillet (2003). Our own results (see section 'Products of crystallization experiments from a basic liquid') complement those of Toplis *et al.* (1994) and Toplis & Carroll (1995) because they were obtained from a starting material very similar to that used by those workers.

As can be seen from Table 7 and Figs 7 and 8, the temperature estimates obtained with our numerical model are encouraging. Eighty per cent of the 39 Tmt–Ilm_{ss} pairs yield temperatures that are within ±50°C of the experimental temperatures. The remaining values are within ±70°C of the experimental values, with the exception of those from one run (Fe-100; Toplis *et al.*, 1994; Fig. 7a). At a first sight, there is an increasing tendency for calculated temperature to be underestimated with decreasing experimental temperatures (Fig. 7a). This could be attributed to the fact that our fits rely heavily on data obtained at $T \geq 1000$°C. However, the question arises whether equilibrium was reached in all the experiments reported by Gardner *et al.* (1995*b*) or Prouteau & Scaillet (2003). The Fe–Ti oxide compositions given by Prouteau & Scaillet (2003) point to considerable inhomogeneities, at least in the titanomagnetites. The 1σ values for X'_{usp} are about 30% of the means of eight or nine single analyses and those researchers listed only single analyses of Ilm_{ss} which may not be representative (Table 7). Gardner *et al.* (1995*b*) provided only means of two to nine single analyses and did not give any standard deviation. The starting materials for their experiments were glass–crystals mixtures that were obtained by hydrothermal annealing of a powdered natural pumice sample at 2 kbar, 825 or 875°C. Although Gardner *et al.* (1995*a*) presented indications that Fe–Ti oxide re-equilibrate within the run durations of 4–5 days at 850°C, the detailed study of Venezky & Rutherford (1999) reveals that significant chemical heterogeneities may persist even after much longer runs. In particular, the latter workers observed that re-equilibration takes longer when P_{H2O} is lower than the total pressure, which holds for all the runs of Gardner *et al.* (1995*b*) listed in Table 7, with one exception (G-3). Venezky & Rutherford (1999) showed that the temperatures calculated from partially re-equilibrated Fe–Ti oxide assemblages may be either lower or higher than the experimental values.

As shown in Fig. 8, our model reproduces the experimental data of Toplis & Carroll (1995) very well and yields much better results than the formulations of Andersen & Lindsley (1988) or Ghiorso & Sack (1991*a*), in particular for low oxygen fugacities. The strongest discrepancies between experimental and modelled temperatures concern the results of a single experiment performed by M. J. Toplis at 1072°C and $\Delta NNO = 0{\cdot}15$ on six different bulk compositions [run products Fe-95 reported by Toplis & Carroll (1995), and Fe-95 to Fe-100 reported by Toplis *et al.* (1994)]. For all compositions the calculations yield underestimates by 40–100°C (Table 7). Interestingly, other models (Andersen & Lindsley, 1988; Ghiorso & Sack, 1991*a*) also consistently produce too low temperatures (Fig. 8), suggesting a possible error in the experimental temperature.

The oxygen fugacity values calculated from the X'_{usp} values and the calculated temperatures generally agree within ±0·4 ΔNNO with the experimental values (Fig. 7b). The values outside this range are essentially correlated with strong underestimates in temperature; that is, the one peculiar experiment of M. J. Toplis discussed above, the results of Gardner *et al.* (1995*b*) and those of Prouteau & Scaillet (2003). In fact, the ΔNNO values reported by Gardner *et al.* (1995*b*) were not measured but, instead, are estimates based on the model of Andersen & Lindsley (1988) combined with the projection scheme of

Downloaded from https://academic.oup.com/petrology/article/49/6/1161/1490007 by guest on 16 August 2022

Table 7: Comparison of experimental temperatures and oxygen fugacities with those calculated with our model from the compositions of coexisting Tmt and Ilm_{ss} in products of experiments from different studies

Reference, sample no.	Tmt n	Tmt X'_{usp} (1σ)	Ilm_{ss} n	Ilm_{ss} X'_{ilm} (1σ)	P (bar)	T_{exp} (°C)	T_{calc} (°C)	ΔT	log $fO_{2\ exp}$	ΔNNO_{exp}*	ΔNNO_{calc1} from $T_{exp} + X'_{usp}$	$\Delta NNO_{calc1} - \Delta NNO_{exp}$	ΔNNO_{calc2} from $T_{calc} + X'_{usp}$	$\Delta NNO_{calc2} - \Delta NNO_{exp}$
Present study														
2.5SC47x4.5	37	0·703 (7)	44	0·922 (5)	1	1082	1048	−34	−10·00	−0·83	−0·63	0·20	−0·78	0·05
2SC47x1.25	49	0·511 (14)	19	0·789 (9)	1	1053	1051	−2	−9·40	0·16	0·53	0·37	0·52	0·36
2SC47x4	21	0·687 (17)	11	0·918 (9)	1	1052	1040	−12	−10·20	−0·62	−0·63	−0·01	−0·69	−0·07
2SC47x6	31	0·729 (6)	9	0·932 (6)	1	1053	1052	−1	−10·51	−0·95	−0·99	−0·04	−1·00	−0·05
Juster et al. *(1989)*														
B11-A	3	0·708	2	0·928	1	1050	1039	−11	−10·45	−0·84	−0·82	0·02	−0·88	−0·04
Snyder et al. *(1993)*														
4-3-86	3	0·723	7	0·921	1	1093	1074	−19	−10·10	−1·07	−0·76	0·31	−0·84	0·23
4-83C-82	1	0·855	6	0·968	1	1108	1088	−20	−11·10	−2·27	−2·13	0·14	−2·23	0·04
Toplis et al. *(1994)*														
Fe-95†	7	0·611	9	0·892	1	1072	1014	−58	−9·16	0·14	0·00	−0·14	−0·25	−0·39
Fe-96	7	0·613	7	0·896	1	1072	1008	−64	−9·16	0·14	0·00	−0·14	−0·29	−0·43
Fe-97	7	0·599	8	0·878	1	1072	1025	−47	−9·16	0·14	0·08	−0·06	−0·12	−0·26
Fe-98	6	0·603	6	0·890	1	1072	1008	−64	−9·16	0·14	0·06	−0·08	−0·22	−0·36
Fe-99	3	0·614	3	0·884	1	1072	1029	−43	−9·16	0·14	−0·01	−0·15	−0·19	−0·33
Fe-100	8	0·581	7	0·900	1	1072	972	−100	−9·16	0·14	0·20	0·06	−0·28	−0·42
Fe-131	5	0·703	5	0·923	1	1072	1047	−25	−10·19	−0·89	−0·68	0·21	−0·80	0·09
Fe-132	8	0·685	6	0·898	1	1072	1081	9	−10·19	−0·89	−0·53	0·36	−0·49	0·40
Fe-133	7	0·700	6	0·926	1	1072	1036	−36	−10·19	−0·89	−0·65	0·24	−0·82	0·07
Fe-136†	8	0·787	8	0·951	1	1072	1063	−9	−10·79	−1·49	−1·48	0·01	−1·53	−0·04
Toplis & *Carroll (1995)*														
Fe-43	12	0·653	5	0·896	1	1096	1049	−47	−9·74	−0·75	−0·19	0·56	−0·38	0·37
Fe-21	11	0·723	5	0·898	1	1095	1127	32	−10·01	−1·00	−0·75	0·25	−0·63	0·37
Fe-47	12	0·707	9	0·916	1	1087	1067	−20	−9·87	−0·77	−0·65	0·12	−0·73	0·03
Fe-51	13	0·698	12	0·910	1	1078	1070	−8	−9·96	−0·74	−0·61	0·13	−0·64	0·10
Fe-49	14	0·675	5	0·900	1	1068	1066	−2	−10·11	−0·74	−0·47	0·28	−0·48	0·27
Fe-52	14	0·715	5	0·910	1	1057	1089	32	−10·32	−0·81	−0·84	−0·03	−0·70	0·11
Fe-70	9	0·808	10	0·956	1	1061	1073	12	−11·21	−1·76	−1·78	−0·02	−1·71	0·04
Scaillet & *Evans (1999)*														
18	8	0·207 (11)	8	0·828 (30)	2238	776	749	−27		1·20	1·58	0·38	1·48	0·28
35	1	0·318	5	0·817 (3)	2088	866	850	−16		0·98	0·92	−0·06	0·84	−0·14
Prouteau & *Scaillet (2003)*														
PIN 100	8	0·175 (50)	1	0·670	9400	750	815	65		4·8	1·86	−2·94	2·07	−2·73
PIN 104	9	0·183 (55)	1	0·680	9600	841	818	−23		2·6	2·06	−0·54	1·99	−0·61
Gardner et al. *(1995b)*														
G-3a	5	0·279	6	0·819	1500	850	815	−35		0·99	1·17	0·18	1·01	0·02
G-3b	5	0·271	4	0·809	1500	850	817	−33		1·09	1·24	0·15	1·09	0·00
G-10a	6	0·258	9	0·810	1500	850	805	−45		0·95	1·36	0·41	1·17	0·22
G-10b	6	0·257	5	0·816	1500	850	800	−50		0·98	1·37	0·39	1·15	0·17
G-8a	6	0·239	5	0·816	1500	850	784	−66		0·71	1·53	0·82	1·27	0·56

(continued)

Downloaded from https://academic.oup.com/petrology/article/49/6/1161/1490007 by guest on 16 August 2022

Table 7: Continued

Reference, sample no.	Tmt n	Tmt X'_{usp} (1σ)	Ilm_{ss} n	Ilm_{ss} X'_{ilm} (1σ)	P (bar)	T_{exp} (°C)	T_{calc} (°C)	ΔT	log $fO_{2\ exp}$	ΔNNO_{exp}*	ΔNNO_{calc1} from $T_{exp}+X'_{usp}$	ΔNNO_{calc1} $-\Delta NNO_{exp}$	ΔNNO_{calc2} from $T_{calc}+X'_{usp}$	ΔNNO_{calc2} $-\Delta NNO_{exp}$
G-8b	3	0·258	5	0·813	1500	850	803	−47		0·91	1·36	0·45	1·16	0·25
G-6a	5	0·248	2	0·829	1500	850	782	−68		0·67	1·45	0·78	1·16	0·49
G-6b	3	0·263	4	0·815	1500	850	805	−45		1·04	1·31	0·27	1·12	0·08
G-15a	6	0·246	3	0·784	2500	850	814	−36		1·19	1·47	0·28	1·32	0·13
G-16a	5	0·208	4	0·782	2500	850	781	−69		0·83	1·83	1·00	1·59	0·76
G-16b	4	0·242	5	0·784	2500	850	782	−68		0·83	1·51	0·68	1·23	0·40

$\Delta T = T_{calc} - T_{exp}$.
*For all 1 bar experiments ΔNNO values are calculated from ΔNNO = log fO_2 (exp) − log fO_2 (NNO) with the values of O'Neill & Pownceby (1993) for the NNO buffer. Otherwise ΔNNO values were given by the researchers. Gardner *et al*. (1995*b*) have calculated ΔNNO from Tmt–Ilm_{ss} pairs.
†Experiments also reported by Toplis & Carroll (1995).

Stormer (1983). In the experiments of Prouteau & Scaillet (2003) problems arose with the monitoring of the oxygen fugacity (B. W. Evans & B. Scaillet, personal communication) with Ni–Pd–NiO and Co–Pd–CoO solid-state sensors (Taylor *et al*., 1992; Pownceby & O'Neill, 1994). The large compositional heterogeneities of the titanomagnetites (see above) translate into large uncertainties in the modelled T–ΔNNO values and may well explain the discrepancies with the experimental values (Table 7, Fig. 7).

In fact, the temperature estimates are sensitive to compositional variations of the Fe–Ti oxide phases. In the products of our crystallization experiments, for example, numerous single EMP analyses (up to 49; see Tables 5 and 7) show variations of the order of only a few per cent, which suggest a reasonable approach to equilibrium ($2\sigma \leq 6\%$ for all oxide concentrations in Tmt and for X'_{usp}; $2\sigma \leq 3\%$ for all oxide concentrations in Ilm_{ss} and for X'_{ilm}; see Tables 5 and 7). With a Monte-Carlo simulation program that generates a hypothetical set of some hundred thousand data points of coexisting titanomagnetite and ilmenite compositions by varying a pair of analyses within their statistical mean error (program 'Oxytemp', Burchard, in preparation), we can show that such small compositional variations induce variations in the estimated temperatures of up to ±60°C. The effect on the ΔNNO estimates is a maximum of ±0·3 log units (Fig. 9).

APPLICATION TO NATURAL ASSEMBLAGES

The thermo-oxybarometer model developed here is designed only for assemblages of titanomagnetite and hemoilmenite (with the $R\bar{3}$ space group) that equilibrated at temperatures above about 700–800°C and low to moderate oxygen fugacities. These conditions restrict the applicability essentially to basic and intermediate magmatic rocks and a few high-temperature metamorphic assemblages. We do not intend here to extensively compare estimates from our model with those of previous formulations. We shall discuss only a few examples from the studies of Fodor *et al*. (1989), Feeley & Davidson (1994), Gardner *et al*. (1995*a*) and Fodor & Galar (1997).

As shown in Fig. 10a, temperature estimates with our model are in some cases very similar to the values obtained from previous models, but may also differ by as much as 90°C. The discrepancies are related both to the model employed previously and to the temperature range. High Mg or Cr contents in the Fe–Ti oxides may also play a role.

One of the datasets represented in Fig. 10 is that of Fodor *et al*. (1989) on Eocene Ti-rich basalts and diabases from the Abrolhos Platform, offshore Brazil. Using the formulation of Buddington & Lindsley (1964), Fodor *et al*. derived temperatures that spread between 650 and 990°C. Our calculations yield similar values, except for the lowest estimate of Fodor *et al*. (650°C) for a core sample of a diabase, which our model shifts to 736°C (Fig. 10a). This value compares better with the other diabase core sample ($T \approx 700$°C with both models).

The temperature values retrieved by Feeley & Davidson (1994) from Andean andesites and dacites using the model of Ghiorso & Sack (1991*a*) are, with one exception, significantly higher than those obtained from our model (Fig. 10a). This reflects the stronger curvature of our isotherms compared with those of Ghiorso & Sack (1991). Consequently, the Ghiorso & Sack model yields temperature overestimates for pairs with X'_{ilm}/X'_{usp} in the range 0·75–0·80/0·15–0·50 (Feeley & Davidson, 1994), but underestimates for pairs with higher X'_{ilm}/X'_{usp} (e.g. Toplis &

Downloaded from https://academic.oup.com/petrology/article/49/6/1161/1490007 by guest on 16 August 2022

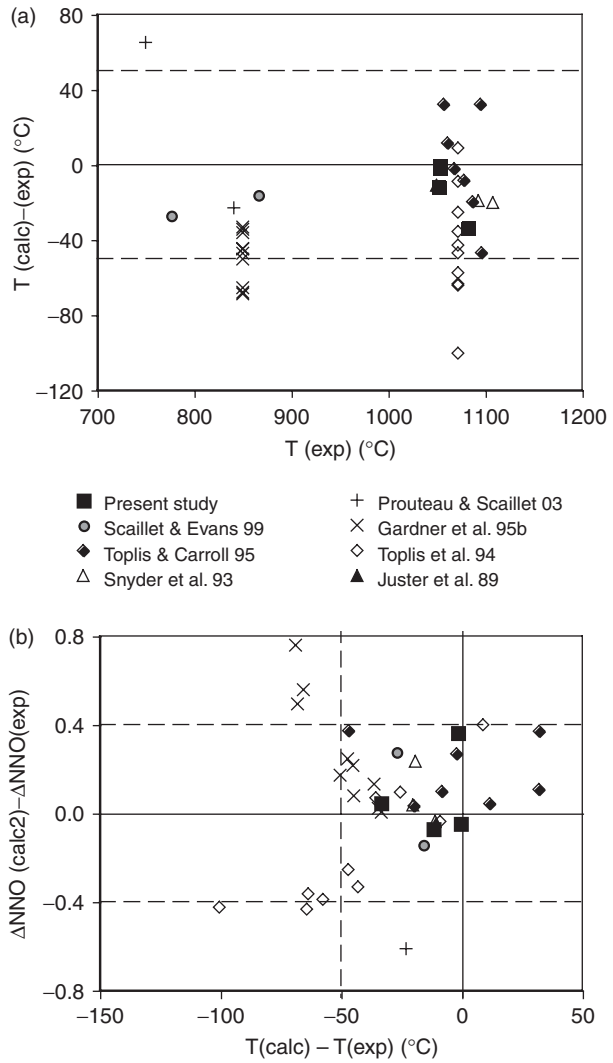

Fig. 7. Differences between T and ΔNNO values calculated with our model (calc) from the compositions of coexisting Tmt and Ilm_{ss} in the run products of selected experimental studies (data sources as indicated) and those reported in the original studies (exp). (a) Temperature differences as a function of the experimental temperatures. (b) Differences between the calculated and experimental ΔNNO values as a function of the difference between the calculated and experimental temperature values. ΔNNO(calc2) refers to ΔNNO values calculated from T(calc) and X'_{usp} (see Table 7). It should be noted that one of the results from Prouteau & Scaillet (2003) plots far outside the diagram (very large difference in ΔNNO).

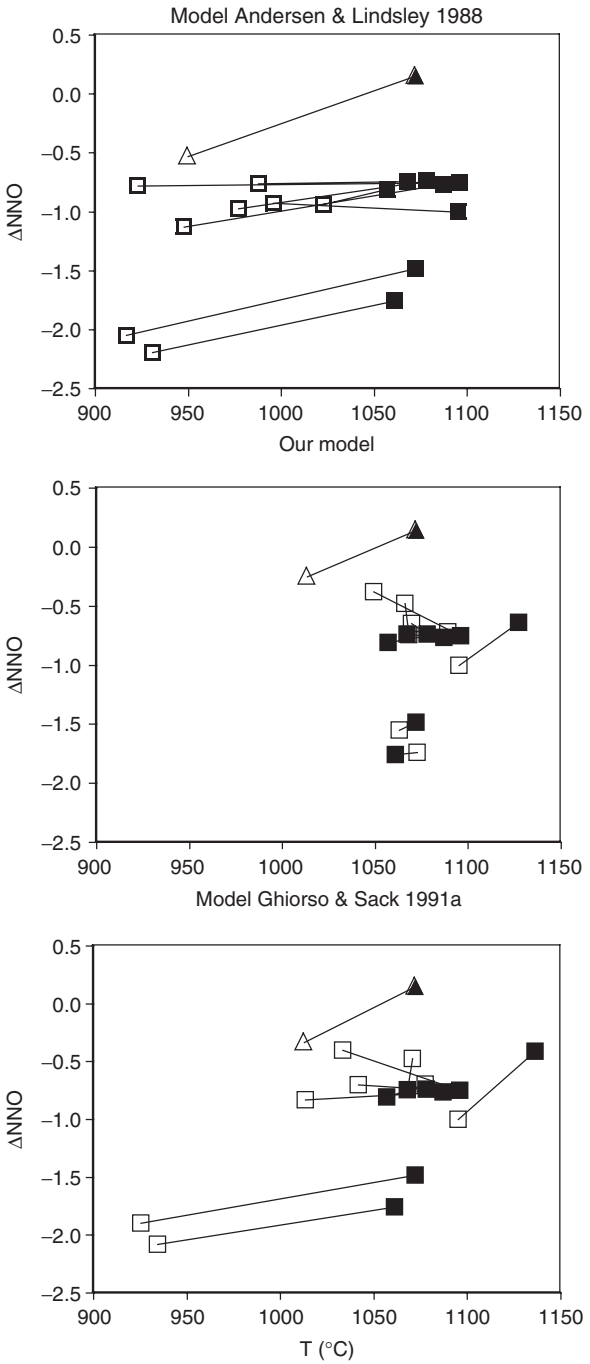

Fig. 8. Comparison between temperature and ΔNNO values (filled symbols) in the experiments of Toplis & Carroll (1995) and those calculated (open symbols) from the composition of coexisting titanomagnetite and $ilmenite_{ss}$ in the run products using either the model of Andersen & Lindsley (1988), or that of Ghiorso & Sack (1991*a*) or our model (ΔNNO calc2; see Table 7).

Carroll, 1995; see Fig. 8). As for the oxygen fugacity estimates, they are not strongly dependent on the model used (Fig. 10b).

Gardner *et al.* (1995*a*) reported analyses of 16 representative Fe–Ti oxide pairs from dacitic pumice clasts of Mount St. Helens. Using the model of Andersen & Lindsley (1988) together with the projection of Stormer (1983), they obtained temperatures in the range 801–912°C and ΔNNO values between 0·8 and 2·0 [recalculated from their original log fO_2 values with the NNO buffer values of O'Neill & Pownceby (1993)]. Gardner *et al.* (1995*a*), however, noted in accordance with Geschwind & Rutherford (1992) that among their temperature estimates those

Downloaded from https://academic.oup.com/petrology/article/49/6/1161/1490007 by guest on 16 August 2022

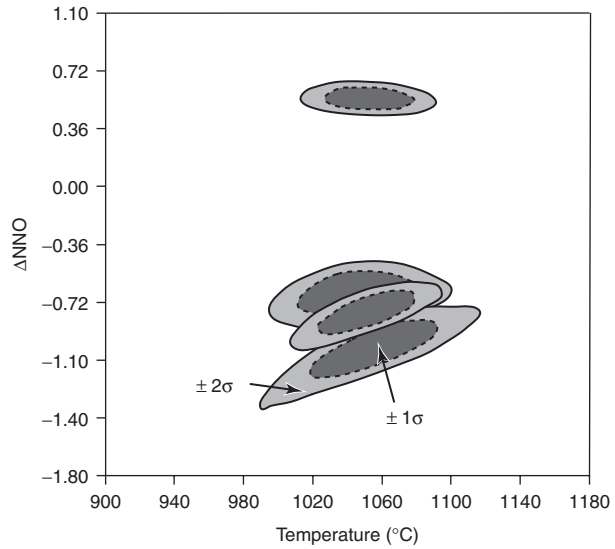

Fig. 9. Influence of statistical uncertainties in the compositions of coexisting titanomagnetite and ilmenite$_{ss}$ in the products of four crystallization experiments (present study; see Tables 5 and 7) on temperature and ΔNNO values calculated with our model. The centre of the elliptical domains represent the T–ΔNNO values calculated from the mean compositions; the dotted curves around the dark parts are the ±1σ boundaries; the continuous curves around the light gray zones are the ±2σ boundaries. The elliptical domains result from a Monte-Carlo simulation with the 'Oxytemp' program (Burchard, in preparation).

correlated with high fO_2 values are too high by about 30°C. In fact, in this T–fO_2 range the formulation of Andersen & Lindsley (1988) is being (mis)-used outside its calibration range and yields temperature overestimates [see discussion by Lattard *et al.* (2005, p. 750)]. Our model lowers these specific T values by 30–40°C, but it also yields lower temperatures by 4–43°C for the other samples of Gardner *et al.* (1995*a*) (Fig. 10a). Our estimated ΔNNO values are in very good agreement—within ±0·2 log units—with those of Gardner *et al.* (1995*a*). At ΔNNO <1·5 our estimates are practically identical to those of the previous model; at higher oxygen fugacities our values are slightly higher (Fig. 10b).

Curiously, Gardner *et al.* (1995*a*) chose to use the formulation of Andersen & Lindsley (1988) on Fe–Ti oxide compositions projected with the scheme of Stormer (1983), although this combination (the so-called 'ALS calibration', e.g. Geschwind & Rutherford, 1992) generally produces higher temperature values than the combination of the Andersen & Lindsley formulation with the projection scheme of the same workers [see examples given by Lattard *et al.* (2005, Fig. 10b)]. Indeed, recalculations with the correct combination [QUILF software of Andersen *et al.* (1993)] give temperatures that are 20–40°C lower than those proposed by Gardner *et al.* (1995*a*) and (with only two exceptions) within ±15°C of our estimates. In any case, arbitrary combinations of thermometer

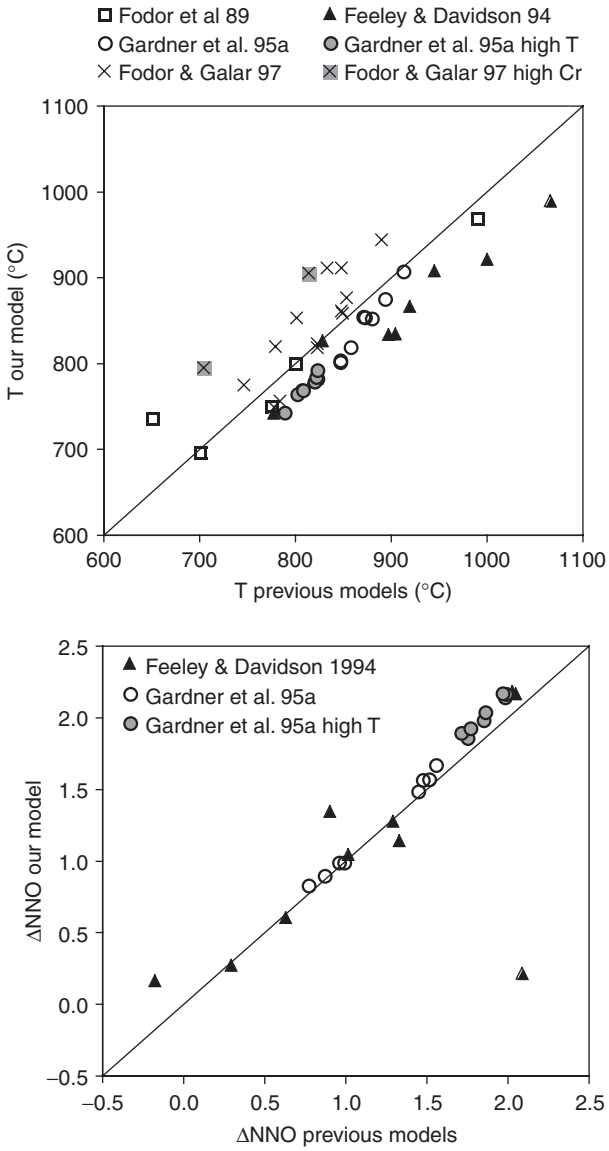

Fig. 10. Comparison of temperature and ΔNNO values retrieved from analyses of coexisting Tmt und Ilm$_{ss}$ in different volcanic rocks either with our model or with previous models; that is, the model of Buddington & Lindsley (1964) with the data of Fodor *et al.* (1989), the model of Ghiorso & Sack (1991*a*) with the data of Feeley & Davidson (1994), the model of Andersen & Lindsley (1988) combined with that of Stormer (1983) with the data of Gardner *et al.* (1995*a*) and an unknown model for the data of Fodor & Galar (1997). Symbols labelled 'high Cr' refer to Cr-rich Fe–Ti oxides, symbols labelled 'high T' refer to temperature estimates considered too high by Gardner *et al.* (1995*a*).

formulations and projection schemes, as listed in the 'ILMAT' Excel worksheet of Lepage (2003), are not recommended.

As a final example, we would like to address the 15 temperature values calculated by Fodor & Galar (1997) for gabbroic xenoliths from Mauna Kea volcano (Hawaii) with an unspecified Fe–Ti oxide model. Fodor & Galar

Downloaded from https://academic.oup.com/petrology/article/49/6/1161/1490007 by guest on 16 August 2022

obtained two slightly overlapping temperature ranges correlating with their sampling sites. Cone-A and cone-B xenoliths yield 704–823°C, cone C xenoliths 801–890°C. Our estimates are in most cases higher (only three exceptions), and the strongest differences appear for samples with Cr-rich titanomagnetites (up to 15·5 wt % Cr_2O_3) that contain also appreciable Mg and Al contents. As we have no experimental data on Cr-rich spinels, it remains unclear whether our temperature estimates are valid for them. Putting the two assemblages with Cr-rich spinels aside, our estimates give more distinct temperature ranges for the two sampling groups: 749–823°C for cones A and B, but 853–944°C for cone C. Our estimates are nearer the values obtained from clinopyroxene–orthopyroxene pairs (953–1087°C) using the geothermometer of Wells (1977).

CONCLUDING REMARKS

The formulation of the titanomagnetite–ilmenite thermo-oxybarometer presented here is based on numerical fits of the temperature and oxygen fugacity dependence of the compositions of coexisting Tmt and Ilm_{ss} of nearly 200 experiments. We considered essentially experiments performed at temperatures in the range 800–1300°C that produced Fe–Ti oxide assemblages with Ilm_{ss} in the space group $R\bar{3}$. Consequently, our formulation of the Tmt–Ilm_{ss} thermo-oxybarometer should definitely not be used if the X'_{ilm} value of the rhombohedral oxide is below that marking the transition between the $R\bar{3}$ and $R\bar{3}c$ structures [see values given by Harrison *et al.* (2000)]. Misuse would yield strong temperature overestimates. It is difficult to decide about the accuracy of our formulation for assemblages equilibrated at temperatures below 800°C because there are only few experimental results in this temperature range and their run products only approached equilibrium. Our calculated isotherms partially match the experimental brackets of Lindsley (1962, 1963) and Spencer & Lindsley (1981) at 600 and 700°C (Fig. 3c), which indicates that our formulation yields at least reasonable approximations for these temperatures.

In the proper T–fO_2 range, tests on independent experimental results have shown that our model reproduces the experimental temperatures within ±70°C, and in most cases within ±50°C. The estimates of the oxygen fugacity are mostly within ±0·4 log units. Compared with the models of Andersen & Lindsley (1988) and Ghiorso & Sack (1991*a*), which yield strong temperature underestimates for assemblages equilibrated at temperatures above 950°C under moderate to low fO_2 values ($\Delta NNO \leq 0$), our formulation performs much better (Fig. 8). This is not surprising because it relies on a strong experimental database and because the effects of minor elements are slight in this T–fO_2 range. This makes our formulation especially reliable for estimates of magmatic T–fO_2 conditions of rapidly cooled intermediate to basic igneous systems. Temperature and oxygen fugacity estimates from Fe–Ti oxides with high contents of additional elements (Al_2O_3, MgO, MnO, $Cr_2O_3 > \sim 6$ wt %) and for those that equilibrated at relatively low temperatures would be better gained from models involving elaborate solid solution models.

ACKNOWLEDGEMENTS

This study was funded by the Deutsche Forschungsgemeinschaft (Grant LA-1164/4-2 and LA-1164/5-3 to D.L.). We thank Hans-Peter Meyer for maintenance of the SEM and EMP laboratories in Heidelberg and for help during the measurements, and Georg Partzsch for preparing the starting glass SC47-P. We gratefully acknowledge helpful discussions with Bernard Evans (Seattle) and the constructive reviews of Hugh O'Neill and Tracy Rushmer. Geoffrey Clarke is thanked for his careful editorial handling.

SUPPLEMENTARY DATA

Supplementary data for this paper are available at *Journal of Petrology* online.

REFERENCES

Andersen, D. J. & Lindsley, D. H. (1988). Internally consistent solution models for Fe–Mg–Mn–Ti oxides: Fe–Ti oxides. *American Mineralogist* **73**, 714–726.

Andersen, D. J., Bishop, F. C. & Lindsley, D. H. (1991). Internally consistent solution models for Fe–Mg–Mn–Ti oxides: Fe–Mg–Ti oxides and olivine. *American Mineralogist* **76**, 427–444.

Andersen, D. J., Lindsley, D. H. & Davidson, P. M. (1993). QUILF: A Pascal program to assess equilibria among Fe–Mg–Mn–Ti oxides, pyroxenes, olivine and quartz. *Computers and Geosciences* **19**, 1333–1350.

Anderson, A. T. (1968). Oxidation of the LaBlache Lake titaniferous magnetite deposit, Quebec. *Journal of Geology* **76**, 528–547.

Buddington, A. F. & Lindsley, D. H. (1964). Iron–titanium oxide minerals and synthetic equivalents. *Journal of Petrology* **5**, 310–357.

Carmichael, I. S. E. (1967). The iron–titanium oxides of salic volcanic rocks and their associated ferromagnesian silicates. *Contributions to Mineralogy and Petrology* **14**, 36–64.

Deines, P., Nafziger, R. H., Ulmer, G. C. & Woermann, E. (1974). Temperature–oxygen fugacity tables for selected gas mixtures in the system C–H–O at one atmosphere total pressure. *Bulletin of the Earth and Mineral Sciences Experiment Station* **88**, 129 pp.

Evans, B. W. & Scaillet, B. (1997). The redox state of Pinatubo dacite and the ilmenite–hematite solvus. *American Mineralogist* **82**, 625–629.

Evans, B. W., Scaillet, B. & Kuehner, S. M. (2006). Experimental determination of coexisting iron–titanium oxides in the systems FeTiAlO, FeTiAlMgO, FeTiAlMnO, and FeTiAlMgMnO at 800 and 900°C, 1–4 kbar, and relatively high oxygen fugacity. *Contributions to Mineralogy and Petrology* **152**, 149–167.

Feeley, T. C. & Davidson, J. P. (1994). Petrology of calc-alkaline lavas at volcan Ollagüe and the origin of compositional diversity at central Andean stratovolcanoes. *Journal of Petrology* **35**, 1295–1340.

Fodor, R. V. & Galar, P. (1997). A view into the subsurface of Mauna Kea volcano, Hawaii: crystallization processes interpreted through

Downloaded from https://academic.oup.com/petrology/article/49/6/1161/1490007 by guest on 16 August 2022

the petrology and petrography of gabbroic and ultramafic xenoliths. *Journal of Petrology* **38**, 581–624.

Fodor, R. V., Mukasa, S. B., Gomes, C. B. & Cordani, U. G. (1989). Ti-rich Eocene basaltic rocks, Abrolhos platform, offshore Brazil, 18°S: Petrology with respect to South Atlantic magmatism. *Journal of Petrology* **30**, 763–786.

Ford, C. E. (1978). Platinum–iron alloy sample containers for melting experiments on iron-bearing rocks, minerals, and related systems. *Mineralogical Magazine* **42**, 271–275.

Frost, B. R. & Lindsley, D. H. (1992). Equilibria among Fe–Ti oxides, pyroxenes, olivine, and quartz: Part II. Application. *American Mineralogist* **77**, 1004–1020.

Gardner, J. E., Carey, S., Rutherford, M. J. & Sigurdsson, H. (1995*a*). Petrologic diversity in Mount St. Helens dacites during the last 4,000 years: implications for magma mixing. *Contributions to Mineralogy and Petrology* **119**, 229–238.

Gardner, J. E., Rutherford, M., Carey, S. & Sigurdsson, H. (1995*b*). Experimental constraints on pre-eruptive water contents and changing magma storage prior to explosive eruptions of Mount St. Helens volcano. *Bulletin of Volcanology* **57**, 1–17.

Geschwind, C.-H. & Rutherford, M. J. (1992). Cummingtonite and the evolution of the Mount St. Helens (Washington) magma system: An experimental study. *Geology* **20**, 1011–1014.

Ghiorso, M. S. (1990). Thermodynamic properties of hematite–ilmenite–geikielite solid solutions. *Contributions to Mineralogy and Petrology* **104**, 645–667.

Ghiorso, M. S. & Sack, R. O. (1991*a*). Fe–Ti oxide geothermometry: thermodynamic formulation and the estimation of intensive variables in silicic magmas. *Contributions to Mineralogy and Petrology* **108**, 485–510.

Ghiorso, M. S. & Sack, R. O. (1991*b*). Thermochemistry of the oxide minerals. In: Lindsley, D. H. (ed.) *Oxide Minerals: Petrologic and Magnetic Significance. Mineralogical Society of America, Reviews in Mineralogy* **25**, 221–264.

Harrison, R. J., Becker, U. & Redfern, S. A. T. (2000). Thermodynamics of the $R\bar{3}$ to $R\bar{3}c$ phase transition in the ilmenite–hematite solid solution. *American Mineralogist* **85**, 1694–1705.

Hemingway, B. S. (1990). Thermodynamic properties for bunsenite, NiO, magnetite, Fe_3O_4, and hematite, Fe_2O_3, with comments on selected oxygen buffer reactions. *American Mineralogist* **75**, 781–790.

Johannes, W. & Bode, B. (1978). Loss of iron to the Pt-container in melting experiments with basalts and a method to reduce it. *Contributions to Mineralogy and Petrology* **67**, 221–225.

Juster, T. C., Grove, T. L. & Perfit, M. R. (1989). Experimental constraints on the generation of FeTi basalts, andesites, and rhyodacites at the Galapagos Spreading Center, 85°W and 95°W. *Journal of Geophysical Research* **94**, 9251–9274.

Lasdon, L. S. & Waren, A. D. (1978). Generalized reduced gradient software for linearly and nonlinearly constrained problems. In: Greenberg, H. J. (ed.) *Design and Implementation of Optimization Software*. Leyden: Sijthoff and Noordhoff, pp. 335–362.

Lattard, D. (1995). Experimental evidence for the exsolution of ilmenite from titaniferous spinel. *American Mineralogist* **80**, 968–981.

Lattard, D. & Partzsch, G. M. (2001). Magmatic crystallization experiments at 1 bar in systems closed to oxygen: A new/old experimental approach. *European Journal of Mineralogy* **13**, 467–478.

Lattard, D., Sauerzapf, U. & Käsemann, M. (2005). New calibration data for the Fe–Ti oxide thermo-oxybarometers from experiments in the Fe–Ti–O system at 1 bar, 1000–1300°C and a large range of oxygen fugacities. *Contributions to Mineralogy and Petrology* **149**, 735–754.

Lattard, D., Engelmann, R., Kontny, A. & Sauerzapf, U. (2006). Curie temperatures of synthetic titanomagnetites in the Fe–Ti–O system: Effects of compositions, crystal chemistry, and thermomagnetic methods. *Journal of Geophysical Research* **111**, B12S28, doi:10.1029/2006JB004591.

Lepage, L. D. (2003). ILMAT: an Excel worksheet for ilmenite–magnetite geothermometry and geobarometry. *Computers and Geosciences* **29**, 673–678.

Lindsley, D. H. (1962). Investigations in the system FeO–Fe_2O_3–TiO_2. *Carnegie Institution of Washington Yearbook* **61**, 100–106.

Lindsley, D. H. (1963). Fe–Ti oxides in rocks as thermometers and oxygen barometers. *Carnegie Institution of Washington Yearbook* **62**, 60–66.

Lindsley, D. H. (1991). Experimental studies of oxide minerals. In: Lindsley, D. H. (ed.) *Oxide Minerals: Petrologic and Magnetic Significance. Mineralogical Society of America, Reviews in Mineralogy* **25**, 69–100.

Lindsley, D. H. & Frost, B. R. (1992). Equilibria among Fe–Ti oxides, pyroxenes, olivine, and quartz: Part I. Theory. *American Mineralogist* **77**, 987–1003.

Lindsley, D. H. & Spencer, K. J. (1982). Fe–Ti oxide geothermometry: Reducing analyses of coexisting Ti-magnetite (Mt) and ilmenite (Ilm). *EOS Transactions, American Geophysical Union* **63**, 471.

O'Neill, H. S. C. (1988). Systems Fe–O and Cu–O: Thermodynamic data for the equilibria Fe–'FeO,' Fe–Fe_3O_4, 'FeO'–Fe_3O_4, Fe_3O_4–Fe_2O_3, Cu–Cu_2O, and Cu_2O–CuO from emf measurements. *American Mineralogist* **73**, 470–486.

O'Neill, H. S. C. & Pownceby, M. I. (1993). Thermodynamic data from redox reactions at high temperatures. I. An experimental and theoretical assessment of the electrochemical method using stabilized zirconia electrolytes, with revised values for the Fe–'FeO', Co–CoO, Ni–NiO and Cu–Cu_2O oxygen buffers, and new data for the W–WO_2 buffer. *Contributions to Mineralogy and Petrology* **114**, 296–314.

Pinckney, L. R. & Lindsley, D. H. (1976). Effects of magnesium on iron–titanium oxides. *Geological Society of America, Abstracts with Programs* **8**, 1051.

Pouchou, J. L. & Pichoir, F. (1985). 'PAP' $\phi(\rho Z)$ procedure for improved quantitative microanalysis. *Microbeam Analysis* **1985**, 104–106.

Powell, R. & Powell, M. (1977). Geothermometry and oxygen barometry using coexisting iron–titanium oxides: a reappraisal. *Mineralogical Magazine* **41**, 257–263.

Pownceby, M. I. & Fisher-White, M. J. (1999). Phase equilibria in the systems Fe_2O_3–MgO–TiO_2 and FeO–MgO–TiO_2 between 1173 and 1473 K, and Fe^{2+}–Mg mixing properties of ilmenite, ferrous-pseudobrookite and ulvöspinel solid solutions. *Contributions to Mineralogy and Petrology* **135**, 198–211.

Pownceby, M. I. & O'Neill, H. S. C. (1994). Thermodynamic data from redox reactions at high temperatures. III. Activity–composition relations in Ni–Pd alloys from EMF measurements at 850–1250 K, and calibration of the NiO + Ni–Pd assemblage as a redox sensor. *Contributions to Mineralogy and Petrology* **116**, 327–339.

Prouteau, G. & Scaillet, B. (2003). Experimental constraints on the origin of the 1991 Pinatubo dacite. *Journal of Petrology* **44**, 2203–2241.

Robie, R. A., Hemingway, B. S. & Fisher, J. R. (1979). Thermodynamic properties of minerals and related substances at 298·15 K and 1 bar (10^5 Pascals) pressure and at higher temperatures. *US Geological Survey Bulletin* **1452**, 456 pp.

Rumble, D. I. (1970). Thermodynamic and analysis of phase equilibria in the system Fe_2TiO_4–Fe_3O_4–TiO_2. *Carnegie Institution of Washington Yearbook* **69**, 198–207.

Sack, R. O. & Ghiorso, M. S. (1991*a*). An internally consistent model for the thermodynamic properties of Fe–Mg-titanomagnetite–aluminate spinels. *Contributions to Mineralogy and Petrology* **106**, 474–505.

Downloaded from https://academic.oup.com/petrology/article/49/6/1161/1490007 by guest on 16 August 2022

Sack, R. O. & Ghiorso, M. S. (1991*b*). Chromian spinels as petrogenetic indicators: Thermodynamics and petrological applications. *American Mineralogist* **76**, 827–847.

Sauerzapf, U. (2006). *New experimental data for a re-calibration of the Fe–Ti oxide thermo-oxybarometers*. Heidelberg: Ruprecht-Karls-Universität, 231 pp.

Scaillet, B. & Evans, B. (1999). The 15 June 1991 eruption of Mount Pinatubo. I. Phase equilibria and pre-eruption P–T–fO_2–f_{H_2O} conditions of the dacite magma. *Journal of Petrology* **40**, 381–411.

Senderov, E., Dogan, A. U. & Navrotsky, A. (1993). Nonstoichiometry of magnetite–ulvöspinel solid solutions quenched from 1300°C. *American Mineralogist* **78**, 565–573.

Snyder, D., Carmichael, I. S. E. & Wiebe, R. A. (1993). Experimental study of liquid evolution in an Fe-rich, layered mafic intrusion: constraints of Fe–Ti oxide precipitation on the T–fO_2 and T–ρ paths of tholeiitic magmas. *Contributions to Mineralogy and Petrology* **113**, 73–86.

Speidel, D. H. (1970). Effects of magnesium on the iron–titanium oxides. *American Journal of Science* **268**, 341–353.

Spencer, K. J. & Lindsley, D. H. (1981). A solution model for coexisting iron–titanium oxides. *American Mineralogist* **66**, 1189–1201.

Stormer, J. C. J. (1983). The effects of recalculation on estimates of temperature and oxygen fugacity from analyses of multicomponent iron–titanium oxides. *American Mineralogist* **68**, 286–594.

Taylor, R. W. (1964). Phase equilibria in the system FeO–Fe_2O_3–TiO_2 at 1300°C. *American Mineralogist* **49**, 1016–1030.

Taylor, J. R., Wall, V. J. & Pownceby, M. I. (1992). The calibration and application of accurate sensors. *American Mineralogist* **77**, 284–295.

Toplis, M. J. & Carroll, M. R. (1995). An experimental study of the influence of oxygen fugacity on Fe–Ti oxide stability, phase relations, and mineral–melt equilibria in ferro-basaltic systems. *Journal of Petrology* **36**, 1137–1170.

Toplis, M. J., Libourel, G. & Carroll, M. R. (1994). The role of phosphorus in crystallisation processes of basalt: An experimental study. *Geochimica et Cosmochimica Acta* **58**, 797–810.

Venezky, D. Y. & Rutherford, M. J. (1999). Petrology and Fe–Ti oxide reequilibration of the 1991 Mount Unzen mixed magma. *Journal of Volcanology and Geothermal Research* **89**, 213–230.

Webster, A. H. & Bright, N. F. H. (1961). The system iron–titanium–oxygen at 1200°C and oxygen partial pressures between 1 atm. and 2×10^{-14} atm. *Journal of the American Ceramic Society* **44**, 110–116.

Wells, P. R. A. (1977). Pyroxene thermometry in simple and complex systems. *Contributions to Mineralogy and Petrology* **62**, 129–139.

APPENDIX

As Supplementary Data to accompany this paper (available for downloading at http://www.petrology.oxfordjournals.org) we provide an Excel file to calculate temperature and oxygen fugacity values from the compositions of coexisting pairs of titanomagnetite and ilmenite$_{ss}$ using our numerical model. Most calculations are performed with the help of macros written in Visual Basic.

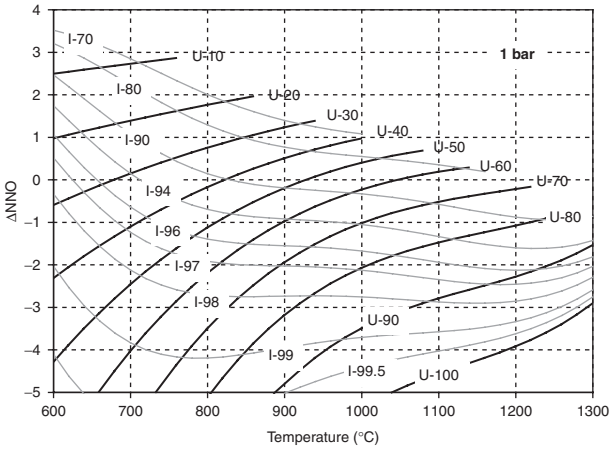

Fig. A1. Isopleths of X'_{usp} (in mol %, black curves) and X'_{ilm} (in mol %, gray curves) as a function of temperature and oxygen fugacity (ΔNNO), calculated using the macros provided in the Supplementary Data Excel file. This figure is similar to a widely used graphical representation of previous versions of the Fe–Ti oxide thermo-oxybarometer (Ghiorso & Sack, 1991*b*).

The file contains nine worksheets. The first worksheet, 'Analyses', can be used to enter the compositions of both phases in term of weight per cent of oxides. The structural formulae (based on stoichiometric titanomagnetite and ilmenite$_{ss}$, with three cations and four oxygens for Tmt, but two cations and three oxygens for Ilm$_{ss}$) are automatically calculated and listed together with the projected mole fractions X'_{usp} and X'_{ilm} in the same column. The user should enter a pressure value and an accuracy for the temperature calculation, which is performed via iteration nesting. The program yields the temperature, ΔNNO and log fO_2 values calculated from the X'_{usp} and X'_{ilm} values. The other worksheets allow the user to set up tables and diagrams involving calculated temperature, ΔNNO, X'_{usp} or X'_{ilm} values. As an example, we show in Fig. Al a plot of X'_{usp} and X'_{ilm} isopleths as a function of temperature and ΔNNO.

It should be stressed that all calculations are valid only with the projection schemes used in the first worksheet [see equation (4a) and (4b) in subsection 'Thermometry']. The users are urged not to use any other projection! The permissible temperature range has been fixed to 600–1400°C. The permissible range of ilmenite compositions is restricted to those in the $R\bar{3}$ space group, which, according to Harrison *et al.* (2000), corresponds to $X'_{ilm} > 0{\cdot}0006\ T + 0{\cdot}095$ (with T in°C).

Downloaded from https://academic.oup.com/petrology/article/49/6/1161/1490007 by guest on 16 August 2022